Marine and Petroleum Geology 78 (2016) 766–784

Contents lists available at ScienceDirect

Marine and Petroleum Geology

journal homepage: www.elsevier.com/locate/marpetgeo

Research paper

Sequence stratigraphy and seismic geomorphology application of facies architecture and sediment-dispersal patterns analysis in the third member of Eocene Shahejie Formation, slope system of Zhanhua Sag, Bohai Bay Basin, China

Qianghu Liu [a, b, **], Xiaomin Zhu [a, b, *], Yong Yang [c], Mingyang Geng [d], Mingxuan Tan [a, b], Long Jiang [c], Liang Chen [d]

[a] Faculty of Geoscience, State Key Laboratory of Petroleum Resources and Processing, China University of Petroleum, Beijing 102249, China
[b] College of Geosciences, China University of Petroleum, Beijing 102249, China
[c] Geological Science Research Institute, Sinopec Shengli Oilfield Company, Dongying 257015, China
[d] China National Offshore Oil Corporation Research Institute, Beijing 100027, China

ARTICLE INFO

Article history:
Received 21 January 2015
Received in revised form
14 November 2015
Accepted 21 November 2015
Available online 2 December 2015

Keywords:
Seismic geomorphology
Stratal slice
Fan-delta
Dispersal pattern
Eocene Sha-3 member
Zhnahua Sag
Bohai Bay Basin

ABSTRACT

An important hydrocarbon reservoir is hosted by the third member of the Shahejie Formation (Es3) in the Zhanhua Sag of the Bohai Bay Basin. Using lithology, wire-line logs and three-dimensional (3-D) seismic data in the southern slope of Zhanhua Sag, we demonstrated the utility of stratal slice images for analyzing facies architecture and sediment-dispersal characters of complex depositional systems in Es3. The Es_3, a para-second-order sequence, can be subdivided into three third-order sequences (from base to top: SQ1, SQ2, and SQ3). The facies architecture was analyzed by using the seismic geomorphology approach based on 3-D seismic data. Sediments of the Es_3 sequences were derived from the southern Chenjiazhuang Uplift via six major incised valleys, four of them associated with slope-break belt in the southern zone, and others in the southwestern zone. Seismic stratal slices reveal different characteristics of the channels and lobes between south and southwest from source to sink. On the basis of an integrated analysis of well log, core data, seismic facies based on multi-seismic attributes, three depositional environments (e.g., "fan-delta", "shallow lacustrine" and "turbidite" facies) have been recognized. Stratal slices indicate that the depositional environments of these sequences evolved from gravel- or sand-rich fan delta and turbidite to lacustrine mud, and lastly to mixed sand-mud fan delta systems. The results of high resolution 3-D depositional systems analysis showed that the third-order sequence located in different systems tracts of the para-second-order sequence would contribute to their systems tracts with the different types and scales of depositional systems. Types of slope belts, subsidence rate, sediment provenance and their evolution jointly control the sediment-dispersal characters in deposition area. The proposed sediment dispersal patterns may aid in the prediction of potential reservoir distribution.

1. Introduction

Sequence stratigraphic concepts have been used to understand the organization of the stratigraphic framework of sedimentary basins (Posamentier and Vail, 1988; Mitchum and Van Wagoner, 1991; Shanley and McCabe, 1994; Cross and Lessenger, 1998; Catuneanu, 2002, 2006). It is also a powerful exploration tool since it characterizes the spatial and temporal distribution of depositional systems, with a component of predictability regarding the distribution and geometry of reservoir, source and seal facies (Shanley and McCabe, 1991; Vail et al., 1991; Catuneanu, 2006; Mancini et al., 2008; Morad et al., 2013). In addition, the relevance of high-resolution sequence stratigraphy to reservoir characterization is evident, as heterogeneities at the scale of outcrops and cores strongly control fluid migration pathways, which are

* Corresponding author. Faculty of Geoscience, State Key Laboratory of Petroleum Resources and Processing, China University of Petroleum, Beijing 102249, China.
** Corresponding author. Faculty of Geoscience, State Key Laboratory of Petroleum Resources and Processing, China University of Petroleum, Beijing 102249, China.
E-mail addresses: lqhchkd@163.com (Q. Liu), xmzhu@cup.edu.cn (X. Zhu).

http://dx.doi.org/10.1016/j.marpetgeo.2015.11.015
0264-8172/

fundamental for hydrocarbon production development (Hampson et al., 2008). The high-order of cyclicity reflects overall depositional trends, while the low-order cyclicity describes the actual changes in depositional trends in details (Catuneanu, 2006). The duration of a third-order sequence that appears in the second-order sequence determines its systems tract portion, which further affects the numbers and sizes of fans. Within the last decade, the most logical workfl follows the transition from seismic stratigraphy, to sequence stratigraphy, to seismic sedimentology (Zeng et al., 1998a, 1998b; Zeng, 2001), seismic geomorphology (Posamentier, 2001). Seismic geomorphology, when used in conjunction with seismic stratigraphy, represents the latest approach to extract stratigraphic insights from 3-D seismic data. It can potentially show more advantage in sedimentary facies description, depositional history or reservoir-scale depositional architecture analysis for subsurface conditions (Posamentier and Kolla, 2003; Posamentier, 2004; Nordfjord et al., 2005; Wood, 2007; Stuart and Huuse, 2012; Dong et al., 2014).

Slope break belts usually constrain the development of specific facies zones, which tended to form the oil and gas accumulation zone, in the depositional systems tracts. And that slope break belts are currently among the most important areas for subtle reservoir exploration (Prather, 2003; Paton et al., 2008; Alfaro and Holz, 2014) and have been hot spots in the exploration of the Bohai Bay Basin (Lin et al., 2000; Li et al., 2002; Feng et al., 2004; Lin et al., 2004; Feng and Xu, 2006; Huang et al., 2012; Chen et al., 2014; Liu et al., 2014). In the latest decade, multivariate analysis was applied in previous study for more accurately characterized geological models in the slope break analysis in Jiyang depression (Huang et al., 2012). But few, if any, addressed the complexity of their dynamic evolution in both transverse space and vertical time with sedimentary architecture evolution in the process of tectonic movements and sediment supplies.

The study area is a hydrocarbon-rich region in the southern Zhanhua Sag (Pang et al., 2014), but the target layers (Eocene Shahejie Formation and Miocene Guantao Formation) are not yet well studied. Especially, the provenance, reservoir elements distribution and its controlling factors restrict the future exploration of the third member of the Shahejie Formation (Es_3) (Wang et al., 2015). In addition, the slope system in the study area has a distinct sequence architecture and sediment filling pattern from south to southwest due to the different extent of subsidence rates, paleo-high locations, paleoflow directions and sediment supplies.

The primary objective of this study is to make a progress in terms of better understanding the overall slope system, in particular the types and distribution of reservoir elements for economic reasons. We interpret available lithology, wire-line logs and 3-D seismic data combing sequence stratigraphy and seismic geomorphology to analyze the valley-slope break system and its control on reservoir distribution from short source-to-sink segments. Besides, we also map the sedimentary facies distribution of the third member of the Shahejie Formation (Es_3) in the systems tract.

2. Geologic setting

Bohai Bay Basin, a large oil and gas province in China, develops in response to compound and complex tectonic events (Zhao and Zheng, 2005). It is located in the east part of North China Craton (NCC). The North China cratonic nucleus consists of Archaean and Proterozoic granites and metamorphic basement, cropping out the west and north of the Bohai Bay Basin. During the Mesozoic and Cenozoic eras, the NCC underwent several distinct phases of rifting and subsidence (Ye et al., 1985), resulting in a large-scale thick Tertiary and Quaternary continental accumulation (Li et al., 2007). The most significant control on extension of Eastern China is widely accepted to be subduction of the Pacific plate beneath the eastern margin of Asia (Watson et al., 1987; Tian et al., 1992; Zhao and Zheng, 2005). Rifting of eastern China persisted from the Late Cretaceous to the Oligocene (Chen et al., 1981; Ma et al., 1983; Ren et al., 2002; Zhao and Zheng, 2005).

The Cenozoic tectonic evolution of the rift basin can be divided into six stages: (1) the initial extensional stage accompanied by red deposits with an eruption of acidic volcanic rocks along major faults (Kongdian Formation deposition period in the Eocene), (2) the extensional rift stage (Member 3 of Shahejie Formation deposition period in the late Eocene), (3) the stable subsidence stage (Member 2 and 1 of Shahejie Formation deposition stage in the Eocene-Oligocene), (4) the contraction stage of decreasing activity of faults (Dongying Formation deposition stage in the late Oligocene), (5) the postrift thermal subsidence depression stage with a normal rate (Guantao Formation in Miocene) and (6) the depression stage with a high subsidence rate (Minghuazhen Formation deposition period in the Pliocene) (Su et al., 2011; Jiang et al., 2013).

The Zhanhua Sag, with an area of 3610 km^2, is a hydrocarbon-rich depression within the Bohai Bay Basin of eastern China (Wang et al., 2005; Hao et al., 2010; Tong et al., 2012). It is bounded by the Chenjiazhuang uplift in the south, and the Yihezhuang-Chengdong uplifts in the north (Fig 1a). Intensive petroleum explorations suggest that petroleum reserves are greater than 19.1×10^8 t (Wen et al., 2009). The basin is a complex Mesozoice Cenozoic faulted basin with a tectonic history involving extension, strike-slip movements and tectonic inversion, amongst other tectonism within a Paleozoic cratonic platform setting (Hou et al., 2001; Shi et al., 2005; Qi and Yang, 2010). The structural development and sequence stratigraphy of the basin mean that the post-Tertiary tectonic evolution of the Bohai Bay Basin can be divided into two stages: a rift stage (from Eocene to Oligocene) and a post-rift stage (from Miocene to Pliocene) (Fig. 2). The rift stage comprises three Paleogene units (Kongdian Formation, Shahejie Formation, and Dongying Formation) and has a stratigraphy generally controlled by boundary faults. The post-rift stage comprises a tectonic sequence of Neogene and Quaternary sediments that occupy the entire basin, and a regional unconformity separates the Paleogene and the Neogene. The present-day Zhanhua Sag consists of a duplex half-graben rift that is influenced by NE–SW and ENE–WSW striking extensional, strike-slip faults. These faults formed multiple low uplifts and half-graben as a gentle slope in the south and faults in the north. Wells drilling into the pre-tertiary basement show that west section of Chenjiazhuang Uplift is composed of Paleozoic marine and marine-terrigenous sediments, and Mesozoic continental volcanic fragment sediments, while the composition of east section is Archean metamorphic basements and Paleozoic marine-terrigenous sediments (Wang, 2005; Peng, 2011).

A major petroleum-bearing stratum of this play type is primarily the third member of the Shahejie Formation (Es_3), the main syn-rift deposits, in the Paleogene. The Es_3 is further divided into three parts, lower, middle and upper part from bottom to top, among which the lower and middle parts have dominated (Wen et al., 2009; Chen et al., 2009; Zhang et al., 2012; Jiu et al., 2013). As the subsidence rate generally exceeded the rate of deposition, a lacustrine basin formed and became wider and deeper. Streams originating from areas of high relief carried clastic sediments towards the basin, where lake-floor fan and turbidite deposit systems formed. The Es3 member is composed of dark-grey and grey mudstones and oil shales in the base, dark mudstones intercalated with a number of small turbidite lenses in the middle, and fluvial-deltaic sandstones near the top (Fig. 2). The lake-floor fans were distributed on both flanks of the lake, and were marked by debris flow and turbidity flow from the edge towards the lake center. On

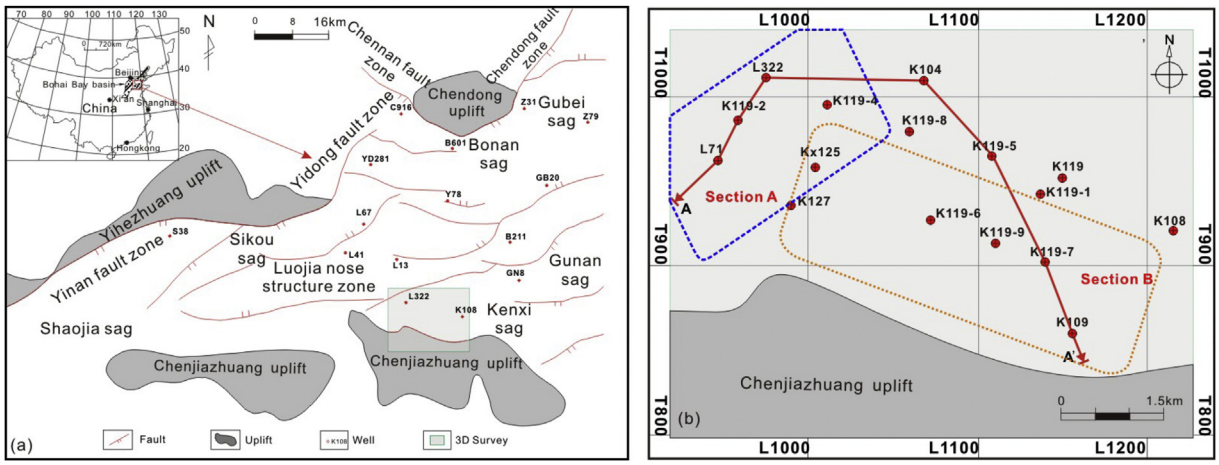

Fig. 1. Study area in the southern slope of the Zhanhua Sag, Bohai Bay Basin. (a) Map shows the elementary structural features of Zhanhua Sag and (b) 3-D seismic surveys and wells used in the study. The red line A–A′ represent seismic lines used in this paper. (For interpretation of the references to colour in this figure legend, the reader is referred to the web version of this article.)

the gentle slope of the faulted depression, several parallels, lake-floor fan groups developed, extending to more than 20–25 km (Zhang et al., 2004).

3. Dataset and methods

The study area is surrounded by the Chenjiazhuang uplift to the south (the major sediment source area), including two types of slopes: gentle slope in the southwestern (Section A) and slope break in the southern (Section B) (Fig. 1b). Based on the well-to-seismic tie for establishing the sequence framework (Fig. 3), the types of slopes can be delineated in the correlation section and a seismic section (A–A′) shown on Fig. 4. The study area for this seismic geomorphology analysis is the 3D seismic surveys (48 km^2), with 16 wells penetrating the study interval. The conventional cores in six wells provide key evidences for sedimentation. The locations of the data used in this study are shown in Fig. 1b.

Poststack 3-D seismic volumes are characterized by an effective frequency range of 0–60 Hz, with a predominant frequency of approximately 33 Hz. The signal-to-noise ratio of the data is relatively high. An excellent well-to-seismic tie was realized using a synthetic seismogram of 16 local wells. Landmark software was used to interpret the 3-D seismic volume, and Recon software was used to generate stratal slices, making it possible to conduct 3-D facies architecture and sediment-dispersal characteristics analysis of the third member of the Shahejie Formation.

The methods of facies architecture and sediment-dispersal patterns analysis used in this study include: (1) sequence framework and fine-scale depositional facies analysis based on 3D seismic profiles and well data; (2) 3D visualization technology analysis for the spatial distribution and temporal evolution of incised valley-slope break systems; (3) seismic multi-attribute analysis for the planar distribution of sedimentary facies with well control; (4) stratal slices from a 3D seismic volume to reveal high-resolution sediment-dispersal patterns in the systems tract; (5) paleogeomorphologic restoration to establish the dispersal pattern of different types of slope depositional systems from source to sink.

4. Sequence stratigraphic and depositional facies analysis

Based on the principles of sequence stratigraphy and taking into account the empirically derived base level and volumetric partitioning and facies variations, we here propose sequence stratigraphic subdivisions for the third member of the Shahejie Formation (Es_3). The Es_3 includes three members from base to top, which is thought to represent a para-second-order sequence with its ascending hemi-cycle comprising the lower and middle members of the Es_3, which is characterized by predominantly coarse-to medium-grained sandstone intercalated with mudstone and regressive sediment sequences. The upper member of the Es_3 coincides with the falling hemi-cycle, which is characterized by mudstone interbedded with sandstone forming progradational sediment sequences (Figs. 2 and 3).

4.1. Sequence stratigraphic analysis

Sequence divisions in the basin are based on regional tectonics, dynamic mechanisms, termination patterns of seismic reflection events, lithology and log data from wells, changes in depositional systems and the geomorphology reflected in the seismic stratal slices.

The well sequence stratigraphic analysis is based on the interpretation of wireline-log patterns and the lithological combinations and successions (Fig. 4), such as (1) sharp lithological contacts (e.g., clean sandstone truncating underlying shale), (2) log curve shape changes (e.g., gamma ray log curves), (3) weathering-denudation surfaces and scouring surfaces, (4) transitional surfaces between the ascending and falling cycles, and (5) thick, widespread mudstone as markers of condensed sections. Based on the interpretation mentioned above, the Es_3 sequence can be further subdivided into three third-order sequences, namely SQ1, SQ2 and SQ3 from base to top, corresponding to three members of the Es_3, which are characterized by cyclically fining-upward to coarsening-upward (Figs. 3 and 4). Sequence SQ1, SQ2, and SQ3 correspond to the lowstand period, the transgressive period and the highstand period respectively. In the seismic section, retrogradational seismic reflections can be seen in sequences SQ1 and SQ2, while it is obvious to observe progradational seismic reflections in sequence SQ3.

In cross-well data (Well-L71 to Well-K109), the strata maintain steady in each sequence, while the sandstone content decreases then increases (Fig. 4a). Sequence SQ1 is primarily made up of thick, coarse-grained sandstone complex in the lowstand systems tract (LST) and the transgressive systems tract (TST), with intercalation of relatively thin mudstone occurring at the top of the TST. The

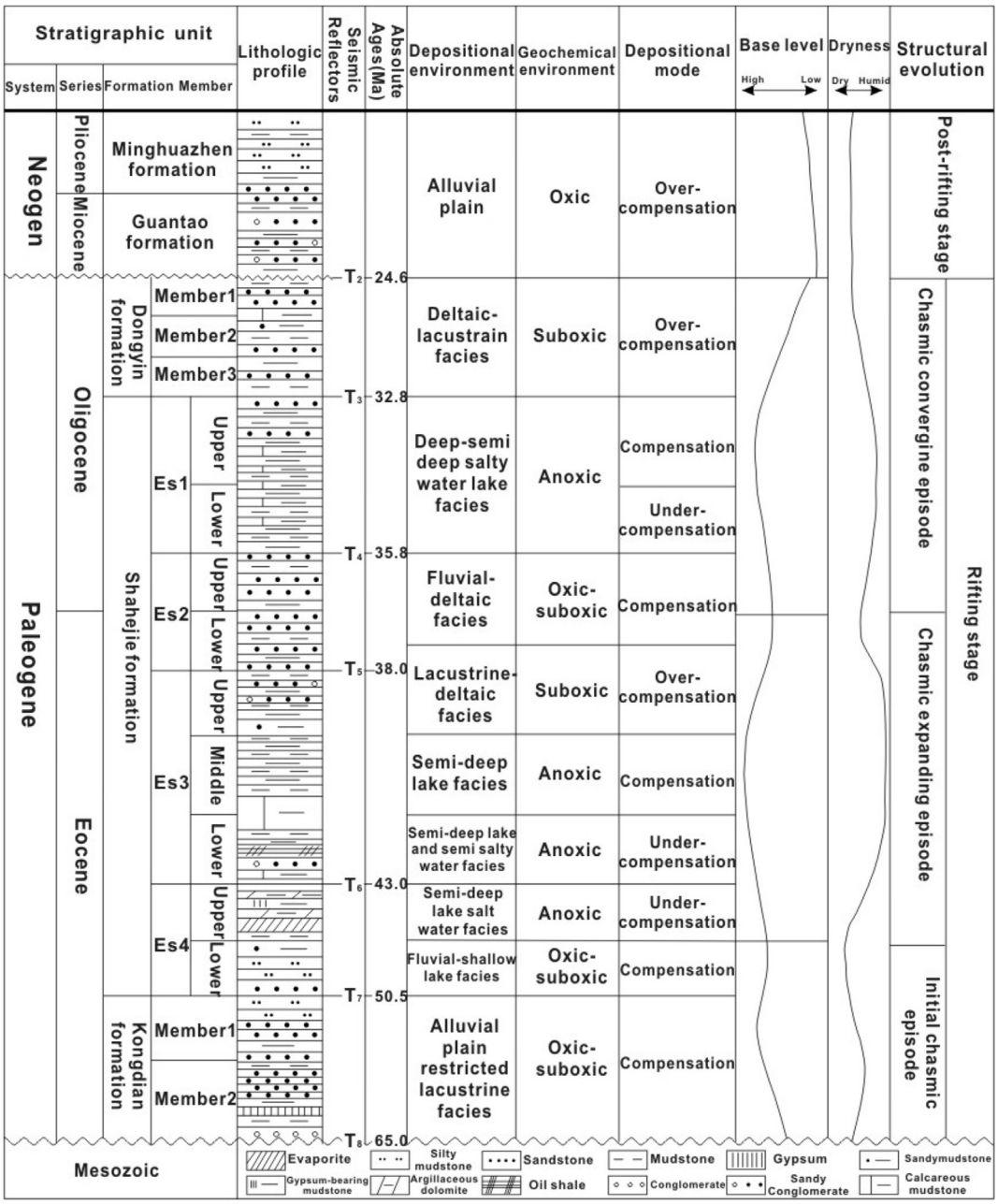

Fig. 2. Generalized stratigraphic column of the Zhanhua Sag showing lithologies, paleoenvironment, base level, dryness, and tectonic evolution (after Zhang et al., 2004; Zhu et al., 2004; Wang et al., 2005; Wen et al., 2009; Jiu et al., 2013). The study interval is the third member of the Shahejie Formation, which was deposited in the extensional rifted stage.

single sand layer of sequence SQ1 becomes thinner and finer grained upward to sandstone in the highstand systems tract (HST). The thickness of the LST and TST in sequence SQ1 is greater than that of HST (Fig. 4a). The sandstone percentage differs considerably between the middle (LST, TST) and the upper (HST) part in both value and distribution (Fig. 4a). For example, the sandstone percentage of the LST and TST varies from 70 to 80% in the southwestern gentle slope zone (Well-L71 to Well-L322), while that of the HST is less and varies between 30 and 35% (Fig. 4a). Meanwhile, the sandstone of the southern slope break zone (Well-K119-7 to Well-K119-5) varies from 40 to 50% in the LST and TST, whereas that of the HST is less and varies between 5 and 10% (Fig. 4a). Sequence SQ2 predominantly consists of multistory mudstone or calcareous mudstone intercalated with thin siltstone beds in the LST and the TST. It becomes thicker and fine-grained in the HST of sequence SQ2. The thickness of the LST and TST in sequence SQ2 is similar to that of HST (Fig. 4a). Sequence SQ3 with interbedded pebble sandstone or fine sandstone and mudstone mainly develops in the HST (Fig. 4a). The sandstone percentage of the HST in Well-L71 to Well-L322 is about 45%, while that of Well-109 to Well-K119-5 is 30%.

From the sequence stratigraphic cross-section shown in Fig. 4a, the stacking patterns of sand-bodies in sequences SQ1, and SQ2 appear to be retrogradational, whereas sequence SQ3 shows progradational stacking patterns. Within sequence SQ1, the sedimentary facies display a distinct retrogradation with a sandstone-dominated lower part and a mudstone-dominated upper part, which invserse in sequence SQ3 (Fig. 4a). The retrogradation or

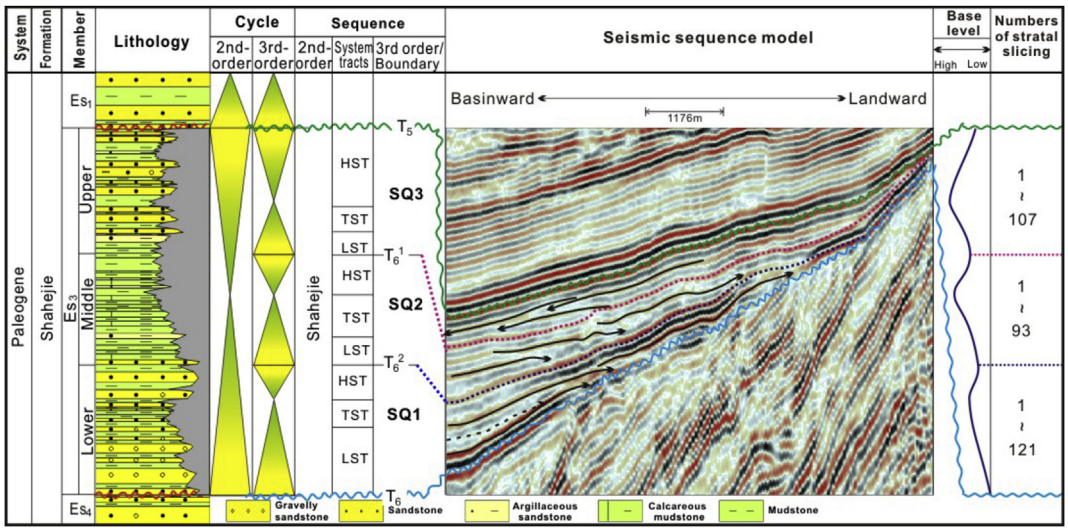

Fig. 3. Enlarged generalized stratigraphic column of the study interval, the third member of the Shahejie Formation, showing lithologies, sequence stratigraphic framework, seismic reflections, and lithology associations.

progradation features and sand-body stacking patterns can be identified along the SW–NE and NW–SE (direction) seismic sections within the SQ1, SQ2, and SQ3 as shown in Fig. 4b. Based on the seismic-lithofacies analysis, the seismic horizons can be traced along the seismic section. From SQ1 to SQ3, the lake level rose and then fell, showing retrogressive landwards to progressive basinwards. This trend is consistent with the sequence stratigraphic correlation from wells and the interpreted spatial distribution of sand-bodies shown in Fig. 4a.

4.2. Well-based facies analysis

Conventional approaches used in well-based sedimentological study generally include core description, lithofacies and logging facies analysis. In this study, there are 16 wells penetrating the study interval (Es_3) and the cores in six wells (eg. Well-K119-2, L322, L71 in the southwestern zone, Well-K119-5, K119 in the southern zone, and Well-Kx125 in the convergence zone) which mainly in sequence SQ1, provides key evidence for deposition.

Fan-delta deposits mostly adjacent to the slope system margin are widely distributed in the Es_3. As in river deltas, fan deltas are characterized by grossly coarsening-upward successions consisting of fan delta plain (subaerial) and fan delta front (subaqueous) subfacies (Fig. 4a) (McPherson et al., 1987, 1988). The subfacies, lithology assemblages and sedimentary structures interpretations are shown in Fig. 5.

Delta-plain deposits developed in the southwestern gentle slope and southern slope break margin, which are mainly composed of (1) thick-bedded conglomerates (Fig. 5b–d,f and g), breccias and pebbly to coarse-grained sandstones with massive or normal graded bedding; (2) interbedded sandstones and red sandy mudstones with massive bedding; and (3) carbonaceous mudstones with horizontal bedding. The coarse-grained lithofacies are interpreted as channel fills and deposits of debris flow on the delta plain, whereas lithofacies (2) and (3) are considered to represent interchannel deposits (McPherson et al., 1988) (Fig. 4a).

Delta-front deposits developed in the outer edge of gentle slope or under the slope break belt, which comprise three major lithofacies: (1) imbricated, graded-to-massive, framework-supported conglomerates with intercalated massive or horizontally laminated sandstones (Fig. 5i–k); (2) thick to thin beds of conglomeratic sandstones and fine-grained to coarse-grained cross-bedded sandstones (Fig. 5l and m); (3) dark, chaotic conglomeratic sandstones containing abundant dark muddy clasts (Fig. 5e), typically associated with slumped or deformed beds; (4) gray to black mudstones and sandy mudstones containing thin-bedded sandstones and conglomeratic sandstones (Fig. 5h). The mudstones are massive or horizontally laminated, while the intercalated fine-grained sand-stones and siltstones display graded bedding and small-scale cross-stratification. Lithofacies (1) and (2), intercalated with dark mudstone, comprise most of the delta-front deposits; these are comparable to subaqueous channel and the mouth bar deposits described by Wood and Ethridge (1988). Lithofacies (3) is interpreted as a subaqueous, debris-flow deposit formed on a delta-front slope (Postma, 1984; Prior and Bornhold, 1988). Lithofacies (4) represent suspension fall-out in the tractive flows or turbidity flows (Orton, 1988).

As the favourable exploration layer, petrographic data of sequence SQ1 in Well-K119-2, Kx125, K119-2, and K119 provides additional information for facies interpretation (Fig. 6). The debris composition of southwestern gentle slope zone is predominantly micritic carbonate rocks with mud-debris structure. The typical sample (from 2188.5 m measured depth (MD) shown in Fig. 6a), which is one of 14 samples analyzed in Well-K119-2, is characterized by poorly sorted and angular grains. Fig. 6b shows the type of debris composed of the carbonate debris and quartz grains in the convergence zone. The sample (from 2188.5 m MD in Well-Kx125) is characterized by variable grains with moderately sorting and roundness. Fig. 6c and d indicates the debris composition of southern slope break zone and the content of quartz or crystal quartz grains increase and play an important role in Fig. 6d (Well-K119). The debris in Fig. 6c and d is characterized by variable grains with moderately sorting and roundness. From Well-K119-2 to Well-K119 (W–E direction), lithology transformed from conglomerate to pebbly sandstone and fine-grained sandstone, and the detrital composition changed from carbonate debris to quartz, which revealed the different provenance and depositional environment between the southwest and south slope system (Figs. 1 and 4a).

5. Facies architecture and sediment-dispersal patterns analysis based on seismic geomorphology

A number of investigations have recently been published on facies architecture analysis based on outcrop, well, seismic, and

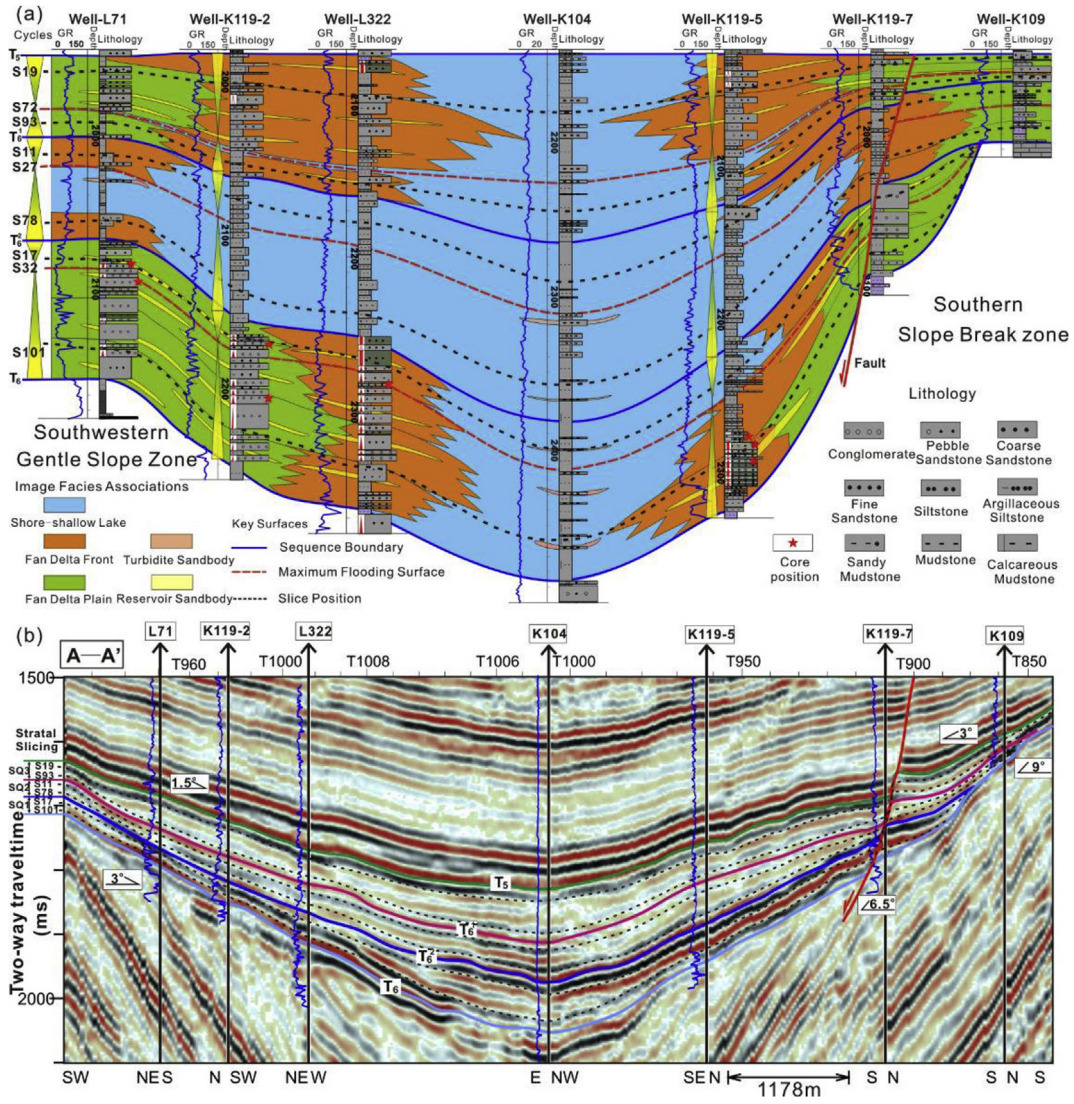

Fig. 4. Cross-well dip seismic section A—A′ showing (a) sequence stratigraphic correlation section from Well-L71 to Well-K104 in the southwestern gentle slope area along SW—NE and Well-K104 to Well-K109 in the southern slope break area along NW—SE including reservoir sand-body distribution of the SQ1, SQ2, and SQ3 sequences; (b) landwards retrogradation of the fan deltas of the SQ1 and SQ2 sequences and basinward progradation of the fan deltas of the SQ3 sequence. See cross-section location in Fig. 1b.

experimental data (Royhan Gani and Mustafa Alam, 2004; Lee et al., 2007; Sech et al., 2009; Sumner et al., 2012; Abdel-Fattah et al., 2013). In this study, seismic geomorphology has been applied to extend the well data study to the entire block covered by 3-D seismic survey and to provide more detailed sedimentary facies architecture mapping (Zeng et al., 1998a, 1998b; Posamentier, 2001, 2002; Carter, 2003; Zeng and Hentz, 2004; Dalla Valle et al., 2013). Using horizontal seismic patterns within a small travel-time window (2~4 ms) that follows the sedimentary facies, a stratal slice can reveal more detailed geomorphology and sedimentary facies in much higher resolution with less ambiguity than that is possible by using classic seismic stratigraphy.

5.1. Rock-physics relationships analysis

The lithology-velocity relationships can be established to predict the lithology in seismic (attribute) profiles effectively through seismic polarity or amplitude. Specifically, Eocene intervals of the study area mainly consist of mudstone, calcareous mudstone, argillaceous siltstone and fine-to coarse-grained sandstone interbedded with pebble sandstone. Fig. 7a shows the crossplot of argillaceous content and P-velocity of the study area, and different colored points in the figure indicate different types of lithology: red points representing sandstone, black points representing mudstone, and green points representing the transitional type between mudstone and sandstone such as argillaceous siltstone. Different colored points are distributed in different velocity-value zones. Generally, sandstone has high P-velocity, and mudstone has low P-velocity. The P-velocities of different lithologies have certain overlaps, and the dividing line of P-velocity value between sandstone and mudstone is around $(3.3–3.7)*10^3$ m/s.

The degree of lithology-decomposition analysis by seismic reflection is also necessary to define whether a single seismic event represents a single lithology or complex lithology (Zeng et al., 2012). In the study area, three third-order sequences have been imaged on seismic profiles and stratal slices, and shows distinctive amplitude patterns. It is very important to establish the relationship between the amplitude pattern and lithology. With a synthetic seismic tie (Fig. 7b), it is inferred that the area of strong negative amplitude (red color) is thick sandstone, whereas the area of weak

Fig. 5. Typical sedimentary structures in third member of Shahejie Formation of the study area. a: mid-fine grained sandstone with small cross bedding, 2085.12 m, Well-L71; b: massive conglomeratic sandstones, 2096.45 m, Well-L71. c and d: thick-bedded massive variegated conglomerates and breccias supported by muddy matrix, 2172.0 and 2206.4 m, Well-K119-2. e: dark, chaotic conglomeratic sandstones containing abundant clasts of mudstone, 2284.0 m, Well-L322. f and g: thick-bedded massive conglomerates and gravels supported by coarse sandy matrix, 2718.5 m, Well-Kx125, located in convergence zone. h: gray mudstones and sandy mudstones containing thin-bedded sandstones with deformation structures, 2277.0 m, Well-K119-5; i: siltstone with low-angle cross-bedding, 2284.6 m, Well-K119-5; j: fine sandstone with parallel bedding, 2296.2 m, Well-K119-5; k: medium-bedded massive positive rhythm fine sandstone, 2297.2 m, Well-K119-5. l and m: fine sandstone with small cross bedding in the upper and siltstone with hummocky cross stratification in the lower, 2258.91–2259 m, Well-K119, located in southern slope break zone.

negative amplitude (lighter-red color) indicates thin sandstone or argillaceous siltstone (Figs. 7c and 8). Positive amplitudes (black color) are interpreted as mudstone beds (Figs. 7c and 8).

5.2. Dispersal characteristics of incised valley-slope break systems

The incised valley developed by deposition or tectonization on the edge of the basin or palaeohigh serves as a channel for sediments delivering and dispersing into the basin. It is usually filled with sandy or gravelly deposits manifested by the bidirectional onlap fill patterns in seismic profiles. So the incised valley fill can be used to identify the sediment transport direction, to deduce the sedimentary dispersal system, and to serve as a potential high-quality reservoir (Wright and Marriot, 1993; Khan and Tewari, 2011; Zhu et al., 2014a,b). In the depositional area, slope break belt limits accommodation variation for basin filling and plays an important role in the development of depositional system and the distribution of sand bodies. Furthermore, sequence style and the range of dispersing sediment are jointly controlled by incised valley and slope break belt.

Four stratal slices (Fig. 8) reveal the paleo-valley time-space migration rules and slope break belt distribution based on the stratal slicing technology in seismic sedimentology and 3D visualization technology, and they can be further deduced matching relationship between the incised valley and sands controlled by slope break belt.

The recognition of common seismic facies is the incised valley fill seismic reflection. A large number of incised valleys can be identified in the Chenjiazhuang Uplift on the seismic data as the cut-and-fill pattern. In Fig. 8, two incised valleys (I and II) were recognized by interpreting the infill patterns in the strike seismic section (XLN798) across the west Chenjiazhuang Uplift, while four incised valleys (III, IV, V and VI) were recognized in the strike seismic section of ILN921. These incised valleys (I and IV particularly) is distinguished by bidirectional onlap fill and progradation fills at different scales. These incised valleys comprise the main drainage system, implying that the sediments from the Chenjiazhuang uplift bypassed the channels before entering the

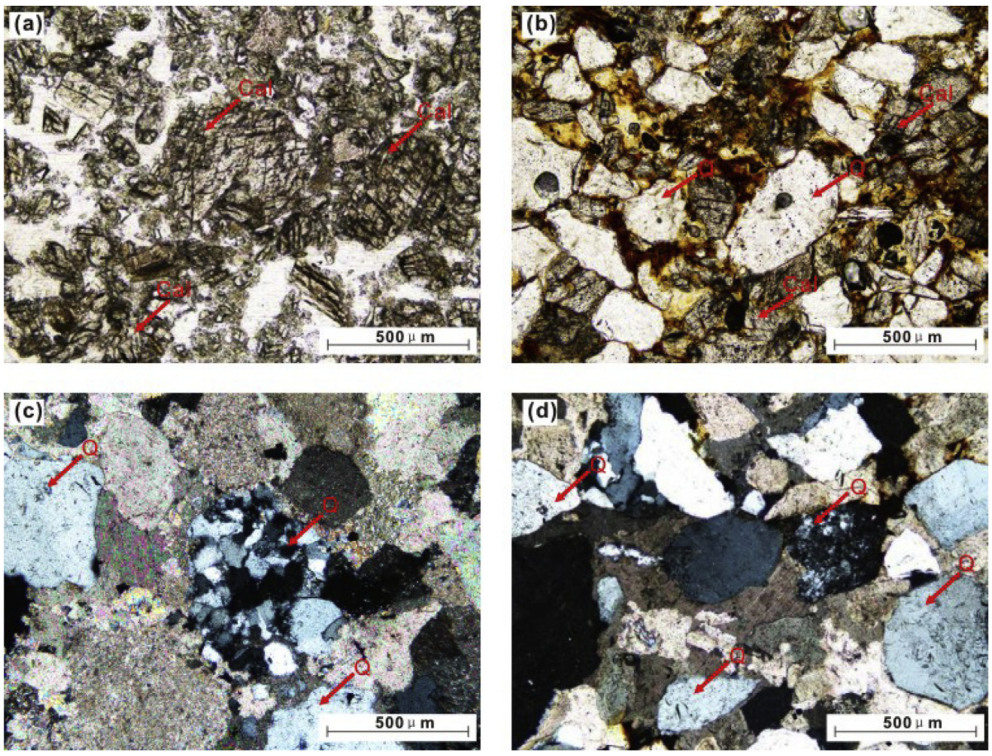

Fig. 6. Representative thin sections from Well-K119-2 to Well-K119 along the W–E direction in sequence SQ1. (a) Thin section at 2188.5 m MD in Well-K119-2 showing carbonates debris with poorly sorted and subangular grains. (b) Thin section at 2292 m MD in Well-Kx125 displaying carbonates debris and quartz grains with moderately sorted and subangular grains. (c) Thin section at 2306.7 m MD in Well-K119-5 showing carbonates debris and quartz grains with moderately sorted and subangular grains. (d) Thin section at 2260.4 m MD in Well-K119 showing quartz grains with moderately sorted and subangular grains.

depositional area.

These stratal slices also indicate the temporal evolution of the incised valley fills and slope break belt from the bottom to the top boundary vividly (Fig. 8). The bottom of each illustration is the stratal slice which shows the reflection amplitude of different stages in the three sequences from Fig. 8a–d. The strong negative amplitudes are characterized by belt-shaped or lobe-shaped distribution.

5.2.1. Temporal evolution of southwestern incised valley system

5.2.1.1. Description. There is no obvious topographic ramp on NE–SW direction (Figs. 4b and 8). In Fig. 8a, the valley I is the main conduit system with the width of 1.3 km on the XLN798 and it has a bigger width-to-thickness ratio (about 12.5, and 104 m thick) than valley II (about 7.4, and 50 m thick) (Time-Depth relationship can be seen in Fig. 7b). The lobe-shaped strong negative amplitude zone develops from valley I with an area of 3.06 km^2 and extends to the well L322. In comparison, in Fig. 8b and the southwestern gentle slope, incised valleys (I and II) are characterized by narrow and separated weak negative amplitude, the zone has decrease and shrink to well-L71 obviously. Fig. 8c shows that the thickness of incised valleys (I and II) have decreased and been dominated by lateral migration in the depositional area. Plate-shaped strong negative amplitude zone (about 10.62 km^2) has extended to the Well-K119-4 and Well-K104 in the southwest. In Fig. 8d, the incised valley I and II fade.

5.2.1.2. Interpretation. The incised valleys (I and II) on the bottom boundary indiacte a strong hydrodynamics for carrying sediments (mainly conglomerate and pebbly sandstone shown in Figs. 4a and 5) with relatively low maturity with moderately sorting and roundness (Fig. 6a). And then, on the top boundary, the down-cutting erosion of incised valleys (I and II) have been weakened and the sediment consists of thin pebbly sandstones intercalated with grey mudstones (Fig. 4a). From Fig. 8a–d, the width and depth (or thickness) variations of incised valleys and the temporal evolution of the incised valley fills from the bottom to top boundary indicate the incised valley system from initiation to extinction.

5.2.2. Temporal evolution of southern incised valley-slope break systems

5.2.2.1. Description. In Fig. 8a, the valley III to VI on the ILN921 has a lower width to depth ratio (about 5.4–10.7, and 47–63 thick) than valley I. Two slope belts exist in the depositional area along the S–N direction (extended distance about 1.76 km). The first-order slope break belt (about 9°, shown in Figs. 4b and 8a) is located in the sedimentary boundary, and the second-order slope break belt (about 6.5°, shown in Figs. 4b and 8a) develops along the direction from Well K119-7, K119-9, K119-6 to Well Kx125. Pieces of lobe-shaped strong negative amplitude zone with an area of 6.54 km2 developed under the direction of the valley III, IV and V between two distinct orders of slope break belt. Several separated lobes with moderate negative amplitude under the second-order slope break belt can reach Well K104. In comparison, in Fig. 8b and the southern slope break belt, incised valleys (III, IV, V and VI) decreased downstream gradually. The paleo-gradient of the first-order and the second-order slope break has reduced to 7° and 5° (Figs. 4b and 8b) respectively. The negative amplitude zone between the slope-break belts (about 8.75 km^2) has retrogressive accumulation. Fig. 8c and d shows that the valleys (III, IV, V and VI) in the south continue to shrink and the slope break belts' gradient has descended to 3° (Figs. 4b and 8d). The valley III to VI corresponds to negative amplitude with a boundary stretching from Well-K104 to the northeast.

5.2.2.2. Interpretation. The width and depth variations of incised

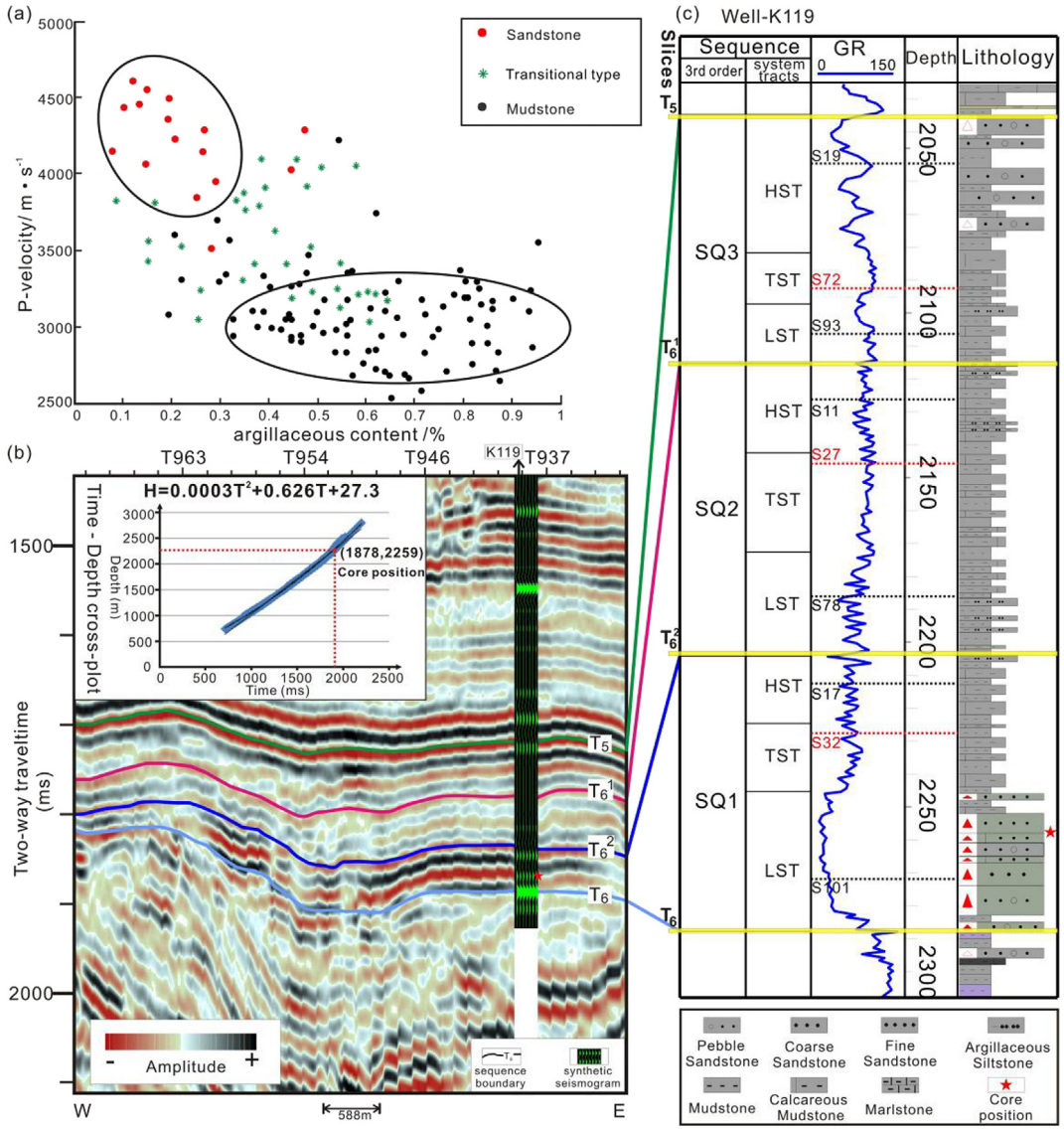

Fig. 7. Rock-physics relationships analysis for Eocene sediments, slope system of Zhanhua Sag. (a) A cross-plot of argillaceous content and P-velocity extracted from wireline-logs (well-L71, L322, K119, K119-5, and K109), (b) (c) lithology correlated with the amplitude pattern in the third member of Eocene Shahejie Formation in well-K119. With a synthetic seismic tie, it is inferred that the area of strong negative amplitude (red color) is thick sandstone, whereas the area of weak negative amplitude (lighter-red color) indicates thin sandstone or argillaceous siltstone. Positive amplitudes (black) are interpreted as mudstone beds. In addition, the time-depth relationship shown in the Fig. 7b, core position in Fig. 7b and c can illustrate it. (For interpretation of the references to colour in this figure legend, the reader is referred to the web version of this article.)

valleys (III, IV, V and VI) in the south similar with valleys (I and II) are under control by slope break system and the distribution of sediments (lithology, sorting and roundness) respectively (Figs. 4a, 5 and 6). On the bottom boundary, they are mainly filled with conglomerate and pebbled sandstone between two distinct orders of slope break belt (Fig. 4a), and mid-fine grained sandstone (moderately sorted and subangular grains) under the second-order slope break belt (Figs. 4a, 5 and 6 and 7). Subsequently, on the top boundary, the sedimentary control of the slope-break belt has weakened, and develops in the entire basin (Fig. 8). The sediments change from pebbly sandstone to fine-grained sandstone or sandy mudstone downstream (Fig. 4a). From Fig. 8a–d, the variations in width and sinuosity of incised valleys and gradients of the slope break belts indicate the evolution of incised valley-slope break systems from initiation to extinction.

5.3. Planar distribution of fans in third-order sequence framework

Seismic multi-attribute analysis can be used to analyze the planar distribution of sedimentary facies for depositional systems analysis with well control. As an assisting tool in seismic interpretation, multi-attribute analysis aims at increasing the interpretation efficiency and the prediction accuracy of seismic attributes, reducing the intuitive uncertainty and multiplicity, and lowering exploration risk (Chopra et al., 2004; Kashihara and Tsuji, 2010; Raeesi et al., 2012; Zhu et al., 2014a, 2014b).

The workflow of multi-attributes starts from sensitivity analysis of each extracted seismic single attribute to evaluate its contribution to improve correlation between seismic signal, lithofacies and logging facies. Then, a supervised clustering was performed to improve the correlation between seismic information and core/log facies. The procedure includes a selection of training data from

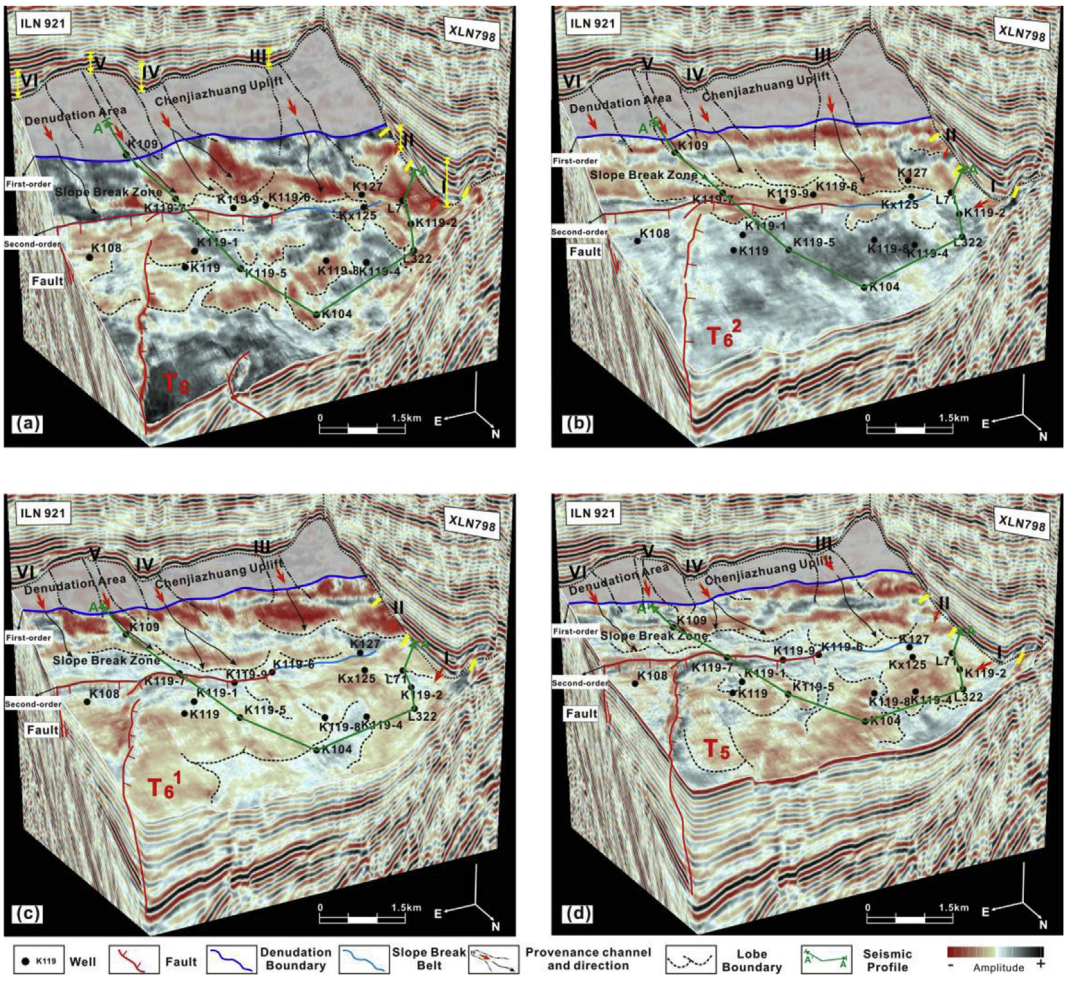

Fig. 8. Stratal slices for seismic amplitude attribute from sequence boundary T_6 to T_5 in the study area showing temporal evolution of the incised valleys, slope break belt, and lobe shape. (a) or T_6: the bottom boundary of sequence SQ1, the main conduit system are valley I in southwest and valley IV in the south; (b) or T_6^2: the bottom boundary of sequence SQ2, the main conduit system are valley III and IV; (c) or T_6^1: the bottom boundary of sequence SQ3, the main conduit system are valley I in southwest and valley IV in the south; (d) or T_5: the top boundary of sequence SQ3, the main conduit system are valley I in southwest and valley IV, VI in the south. The orientation of figure can be seen in the lower right corner. The seismic profile A–A′ can be seen in Fig. 4b.

core- and wireline log-calibrated seismic data near bore hole, followed by neural network classification using a back propagation algorithm. As a result, multiple single attributes are combined to produce a seismic facies classification map (James et al., 2002; Coleou et al., 2003).

In this study, three single attributes, an amplitude attribute of root mean square (RMS), an instantaneous attribute of instantaneous frequency (IF) and a spectral attribute of bandwidth (BW), were found with some power to individually distinguish depositional facies. These attributes, which termed as a seismic facies classification index, were combined to form one new attribute by using a supervised neural network classification method (Raeesi et al., 2012) with calibration with well data (Figs. 4a, 5 and 7). In the resultant seismic facies classification maps (Figs. 9a, 10a and 11a), three types of facies are identified based on supervised learning for nonlinear relationship between sandstone content and the seismic attributes near the bore hole. The red facies indicates sand-rich sediments; the blue facies represents mud-rich sediments; and the yellow facies is a transitional facies containing mixed sandstone and mudstone. A final interpretation of depositional facies could be made on the basis of these seismic facies, supplemented by vertical seismic facies analysis (Figs. 4b and 7) and the distribution on amplitude stratal slices (Fig. 8), and calibrated by well-based sedimentological analysis (Figs. 4a, 5 and 6 and 7).

5.3.1. Sediment patterns in sequence SQ1

Due to the transition from arid to humid paleoclimate during the deposition of sequence SQ1 (Zhu et al., 2004; Zhang et al., 2004), the study area experienced maximum tectonic subsidence and the constantly rising lake level, and the accommodation space at the root of slope system also increased resulting in the transportation of sediments from the Chenjiazhuang Uplift by the incised valleys. After that, the sediments entered into the depositional area, and then rapidly accumulated at the root of the gentle slope belt in the southwest or the slope break belt in the south.

On the seismic multi-attribute map of sequence SQ1 (Fig. 9a), the red and yellow facies dominantly manifest fan-shaped distributions with different scales at the root of the slope systems. Depositional facies maps are made, according to the lithofacies definition of each colored facies (Fig. 9b). Well-based sedimentological characteristics at Well-L71 to Well K109 show that the sandbodies of sequence SQ1 are mainly composed of several finning-upward cycles interpreted from the wireline-log patterns, the lithological associations, and core description (see Figs. 4a and 5). The well-seismic tie shows retrogradational stacking patterns at

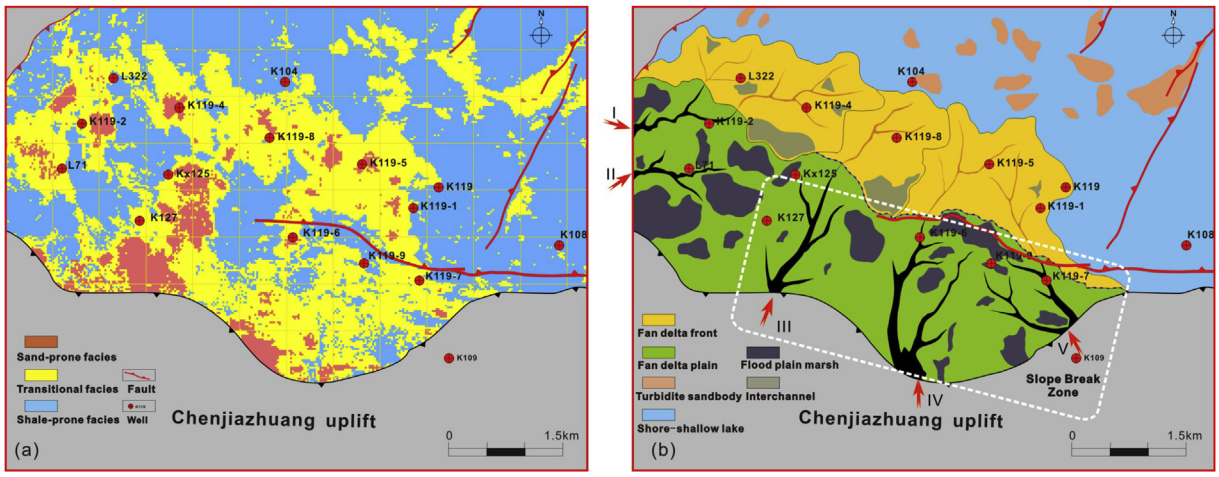

Fig. 9. Seismic facies classification map (a) and interpreted sedimentary facies map of SQ1 (b).

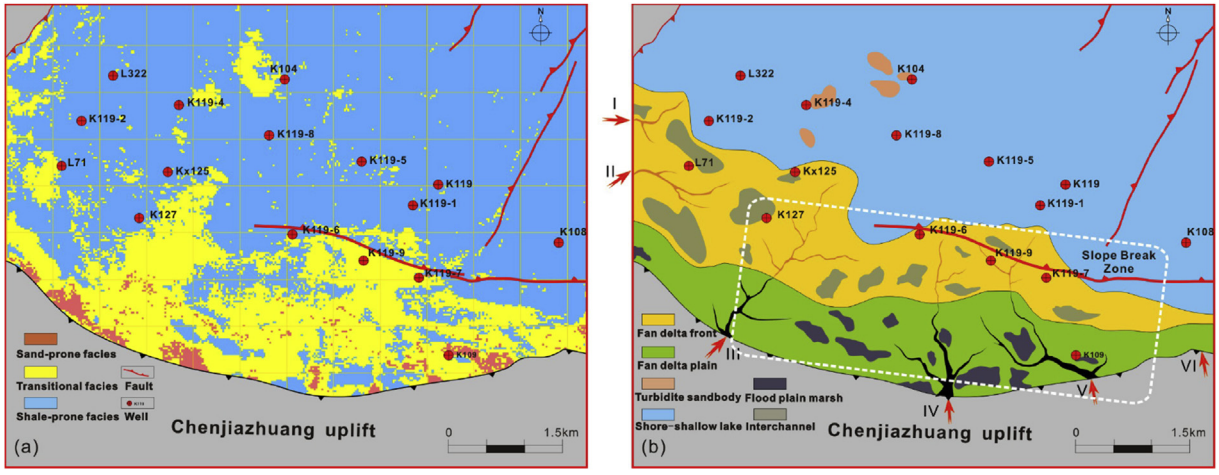

Fig. 10. Seismic facies classification map (a) and interpreted sedimentary facies map of SQ2 (b).

the Well-K119-2 and Well-K119-5 (Fig. 4). The well-based sedimentary facies, seismic facies, and seismic sedimentology-derived facies architecture collectively indicate that the fan-shaped or lobate seismic multi-attribute anomalies (e.g., red and yellow facies) are rapidly accumulated proximal fan-deltas.

The southwestern fan, which is controlled by the mainly source from valley I and the gentle slope belt, is a typical gravel-rich fan-delta system with the red and yellow facies located between the Well-L71 and Well-K119-4. The fan in the southwest is characterised by low gradient (2.6–3.0°, shown in Figs. 4b and 8), admixtures of muddy debris and pebbly conglomerates and poor reservoir quality (Figs. 4a, 5 and 6a). Furthermore, the southern fans, which is controlled by two orders of slope break belts, are sand-rich fan-delta systems located along the Well-K127 to Well-K119-5, corresponding to lobate red and yellow facies dominated by relatively high gradient (5.8–7.0°, shown in Figs. 4b and 8a). These fans are generally composed of mid-fine grained sandstones with good reservoir quality (Figs. 4a, 5–7c). In the northern part of the study area, most blue areas are interpreted as shallow lacustrine facies associated with several turbidite sandbodies (Figs. 4a and 9b).

5.3.2. Sediment patterns in sequence SQ2

Because of the humid climate during the deposition of sequence SQ2 (Zhu et al., 2004; Zhang et al., 2004), base level continued to rise and reached the maximum, leading to the drowning part of the Chenjiazhuang Uplift which has been a depositional area. Base-level rise caused its surface to move landward, enlarging the area of positive accommodation space and thus increased the sediment storage capacity toward the land.

On the seismic multi-attribute map of sequence SQ2 (Fig. 10a), the red and yellow facies cover the part of Chenjiazhuang Uplift, revealing that sediments shifted landward and migrated across the second-order slope break belt. The fan-shaped seismic multi-attribute anomalies still can be observed at the root of the slope system the similar with sequence SQ1, although an increase in the volume of sediments accumulated on the Chenjiazhuang Uplift reduces them available for down-slope transport and accumulation in the basin. Similarly, the multi-attribute anomalies (red and yellow facies) that occur between two distinct orders of slope belts are believed to have been formed in a mud-rich fan deltaic depositional environment (Fig. 4a).

The punctate seismic multi-attribute anomalies developed under the southwestern gentle slope are interpreted as fan delta front corresponding to the valley I and II (Figs. 4a, 8b and 10b). The fan-shaped or lobate seismic multi-attribute anomalies developing between the southern slope break belts are interpreted as fan delta (Fig. 4a). The subfacies transform from fan delta plain in Well-109

to fan delta front in Well-k119-7 corresponding to the valley III, IV and V (Figs. 4a, 8b and 10b). The blue or muddy facies in the northern part of the study area are interpreted as shallow lacustrine facies extending with five isolated turbidite sandbodies (Figs. 4a and 10b).

5.3.3. Sediment patterns in sequence SQ3

Opposite to the tendency of paleoclimate during the deposition of sequence SQ1 (Zhu et al., 2004; Zhang et al., 2004), the base level began to fall continuously and tectonic activities weakened gradually, causing the Chenjiazhuang Uplift to be a source area during the deposition of sequence SQ3. Available accommodation zone shifted basinward so that more sediments can be transported basinward when lake-level fell (Coe et al., 2003). More sediment bypassed through the Chenjiazhuang Uplift, accumulating at the root of the slope system. As a result, the fan-shaped red and yellow seismic facies multi-attribute was distributed in the southwestern gentle slope zone and the southern slope break zone (Fig. 11a). This sequence is mainly dominated by mixed sand-mud fan delta (Figs. 4a and 7c).

On the seismic multi-attribute map of sequence SQ3 (Fig. 11a), the red and yellow facies located at the root of the slope system display fan-shaped distributions predominantly. More sediments in the sequence SQ3 were accumulated toward the basin center after long-distance transportation compared to the seismic multi-attribute distribution of sequence SQ1 and SQ2. Thus, the large-scale progradational seismic reflections (Figs. 3 and 4b), seismic sedimentology analysis (Figs. 4a and 7c), and the fan- or plate-shaped seismic multi-attribute anomalies are interpreted as fan deltaic deposition.

Along the planar distribution of multiple incised valleys, the delta-plain deposits with the red and yellow facies develop at the edge of the slope, while the delta-front deposits of fan deltas with the yellow facies develop in the outer edge of gentle slope or under the slope break belt (Figs. 4, 7c, 8c, d and 11b). The mud-prone area, shown by blue anomalies in the northern part of the study area, is believed to be shallow lacustrine facies with shallow depth (Figs. 4a and 11b). Seismic multi-attribute anomalies change from red (sandy) facies from the edge to the basin center, through yellow (transitional) facies, to blue (muddy) facies, reflecting a general decrease of sand content.

According to the sedimentary systems analysis, medium-scale fan deltas developed in the northwestern and northern slope margin of the study area in the sequence SQ1. In the sequence SQ2, tectonic activity weakened and kept stable. As the extent of the lake expanded, the scale of the fan delta system gradually atrophied, and small-scale turbidite sandbodies developed. During the sequence SQ3, as the lake range reduced, the scale of the fan delta expanded again, and large-scale fan delta systems were formed.

5.4. Seismic mapping of high-resolution sediment-dispersal patterns

Seismic amplitude patterns on the stratal slices provide critical lithologic and geo-morphologic information for sedimentary microfacies analysis. Viewing stratal slices through relative geologic time offers a unique approach to study the systems tracts at relatively high resolution. The total numbers of stratal slices are 321. Among them, the number in SQ1 is 121, 93 in SQ2, and 107 in SQ3 (Fig. 3).

In the study area, several stratal slices from LSTs, TSTs and HSTs of the three sequences SQ1, SQ2 and SQ3 reveal the spatial and temporal evolution of fans in the slope system (Figs. 12–14). With well-to-seismic integrate calibration, the relationship between the amplitude pattern and lithology has been established. It's inferred that the area of strong negative amplitude (red color) is thick sandstone and conglomerate, while the area of weak negative amplitude (lighter-red color) indicates thin sandstone or muddy sandstone (Figs. 4, 7, 8, 12, 13, and 14). Positive amplitudes (black) are interpreted as mudstone beds (Figs. 4, 7, 8, 12, 13, and 14).

5.4.1. Seismic mapping of sequence SQ1

Based on the lithology and well logging analysis, SQ1 is interpreted as fan delta, including distributary channels and flood-plain marshes in delta plain subfacies, subaqueous distributary channels, interchannels, and distributary mouth bars in delta front subfacies (Figs. 4a and 5). Fan deltas are roughly lobe-shaped in plane view and wedge-shaped in cross section. Fig. 12 shows the typical stratal slices of LST, TST and HST in sequence SQ1. The sediment provenances for the study area are the Chenjiazhuang Uplift to the southwest and south (Fig. 8a).

During the LST, a large volume of sands and gravels deposited as lowstand deltas. The gravel-rich fan delta in the gentle slope belt with an area of 6.23 km^2 had a close corresponding relationship with valley I and II, while the sand-rich fan deltas corresponding to valley III, IV, V and VI (mainly of IV and V) in the south had a total area of 12.75 km^2. The positive amplitude anomolies in the central area corresponded to shore-shallow lake subfacies with 3–4 isolated turbidite sandbodies (Fig. 12a, a′). Then, as sediment supply decreased in TST, fan deltas in southwestern and southern area

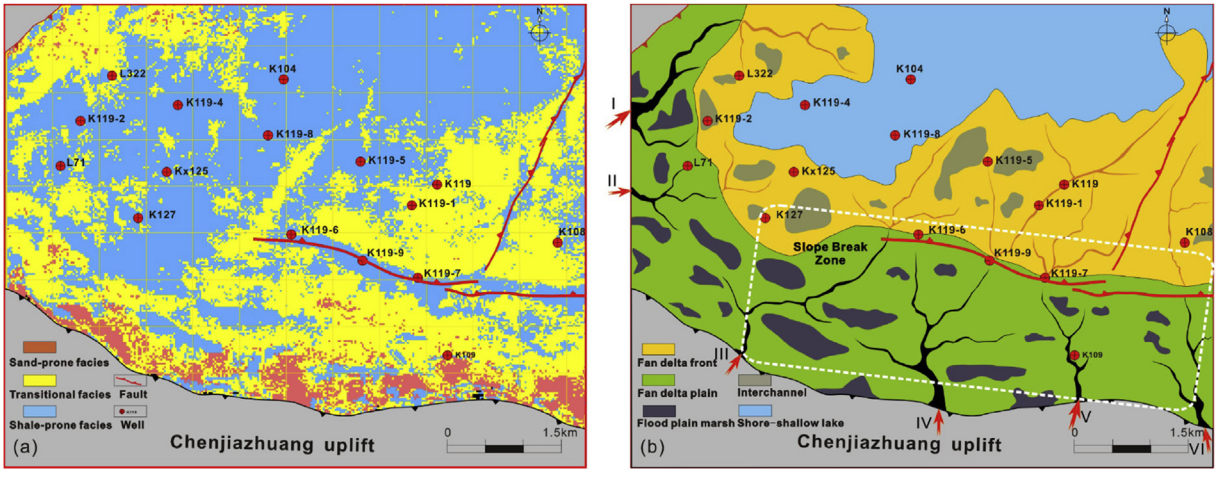

Fig. 11. Seismic facies classification map (a) and interpreted sedimentary facies map of SQ3 (b).

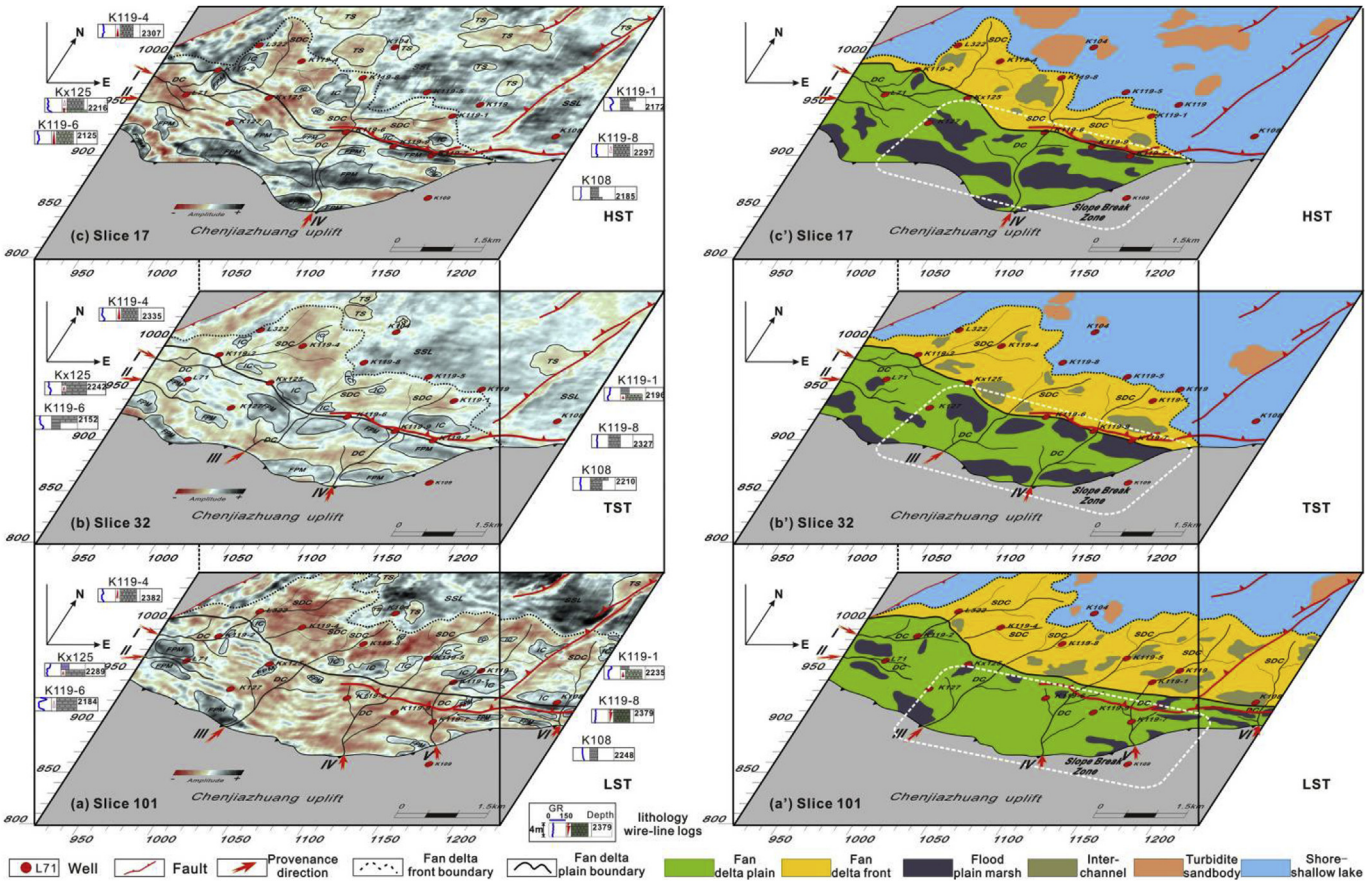

Fig. 12. Three representative stratal slices from SQ1 showing the geomorphologic pattern of the gravel- or sand-rich fan deltaic system. SSL = shore-shallow lake; TS = turbidite sandbody; SDC = subaqueous distributary channel; IC = interchannel; DC = distributary channel; FPM = flood-plain marsh. The time-interval of each slice is 4 m. (a) Slice 101; (b) Slice 32; (c) Slice 17. See Fig. 4 and 7c to locate the stratal slicings.

reduced to 5.65 km^2 and 8.12 km^2 respectively with significantly decreased sandstone content. In this period, the shore-shallow lake enlarged obviously, which complied with four turbidite sandbodies (Fig. 12b, b′). At the HST, sediment supply continued to decrease, and the thickness and distribution of sandstones decreased. The mixed sand-mud fan in the southwest decreased to 4.92 km^2, and the mud rich fan deltas in the south continued to shrink with an area of 7. 56 km^2 mainly controlled by valley IV. There were 5–6 different sized turbidite sandbodies with a maximum area of 0.62 km^2 deposits in front of the fan delta. Meanwhile, the shore-shallow lake enlarged continuously (Fig. 12c, c′).

Within sequence SQ1, fan-shaped negative amplitude mainly developed in the lowstand period with the fan size decreasing from the lowstand to the highstand periods. Especially, fan delta front subfacies controlled by the second-order slope break belt in the south reduced significantly. The fan delta changed from sand/gravel-rich to mixed sand-mud, mud-rich from LST to HST. Fan delta front subfacies were richer in sandstone content and better connectivity than fan delta plain subfacies, while turbidite sandbodies mainly developed in the HST. The favourable reservoirs in the study are mainly located in the two zones, which the delta front subfacies of HST in the northwest and LST under the second-order slope break belt in the south. The characteristics of oil in drilled wells (e.g., Well-L322 and K119-5) could define the rationality.

5.4.2. Seismic mapping of sequence SQ2

Sediments of SQ2 were deposited mainly in a fan delta subfacies, including subaqueous distributary channels, interchannels, distributary bars and sheet sandbodies (Fig. 13). The main sandbodies are thinner, lower-porosity sheet sandbodies. Fig. 13a, b and c shows typical stratal slices of LST, TST and HST in SQ2.

During the LST, sediment supply in the southwest was restrained (mainly by valley II), and the mud-rich fan delta front subfacies shrunk to the area of 2.72 km^2. Under the control of the incised valley III, IV and V in the south, the fan deltas were distributed on the slope platform, with the area of 8.48 km^2. There were four small to medium slump turbidite developed in front of the fan with the area about 0.05–0.25 km^2 (Fig. 13a, a′). Then, the mud-rich fan deltas, which were mainly located between the slope break belts with the area of 7.56 km^2 continued to dwindle associated with small slump turbidite in the front of the fan (Fig. 13b, b′). At the Highstand, the thickness and distribution of sandstones increased due to the increasing sediment supply. The area of fan delta slightly expanded, mixed sand-mud lobes of the fan delta front facies in the south extended to the Well-K119-5 and Well-K119, with the area of 9.02 km^2. Five slump turbidite with the area of 0.08–0.25 km^2 developed near the Well-L322 and K104 at this period (Fig. 13c, c′).

Within sequence SQ2, the lake rarely changed and the number and size of fans almost kept the same in the LST and HST. The sizes of fans reduced and were mainly located between two distinct orders of slope belts. Fan delta front subfacies were richer in sand and showed better connectivity than fan delta plain subfacies, while turbidite sandbodies are primarily distributed in front of the fan body. What's more, the SQ2 is favourable hydrocarbon source rocks interval in the third member of Shahejie Formation.

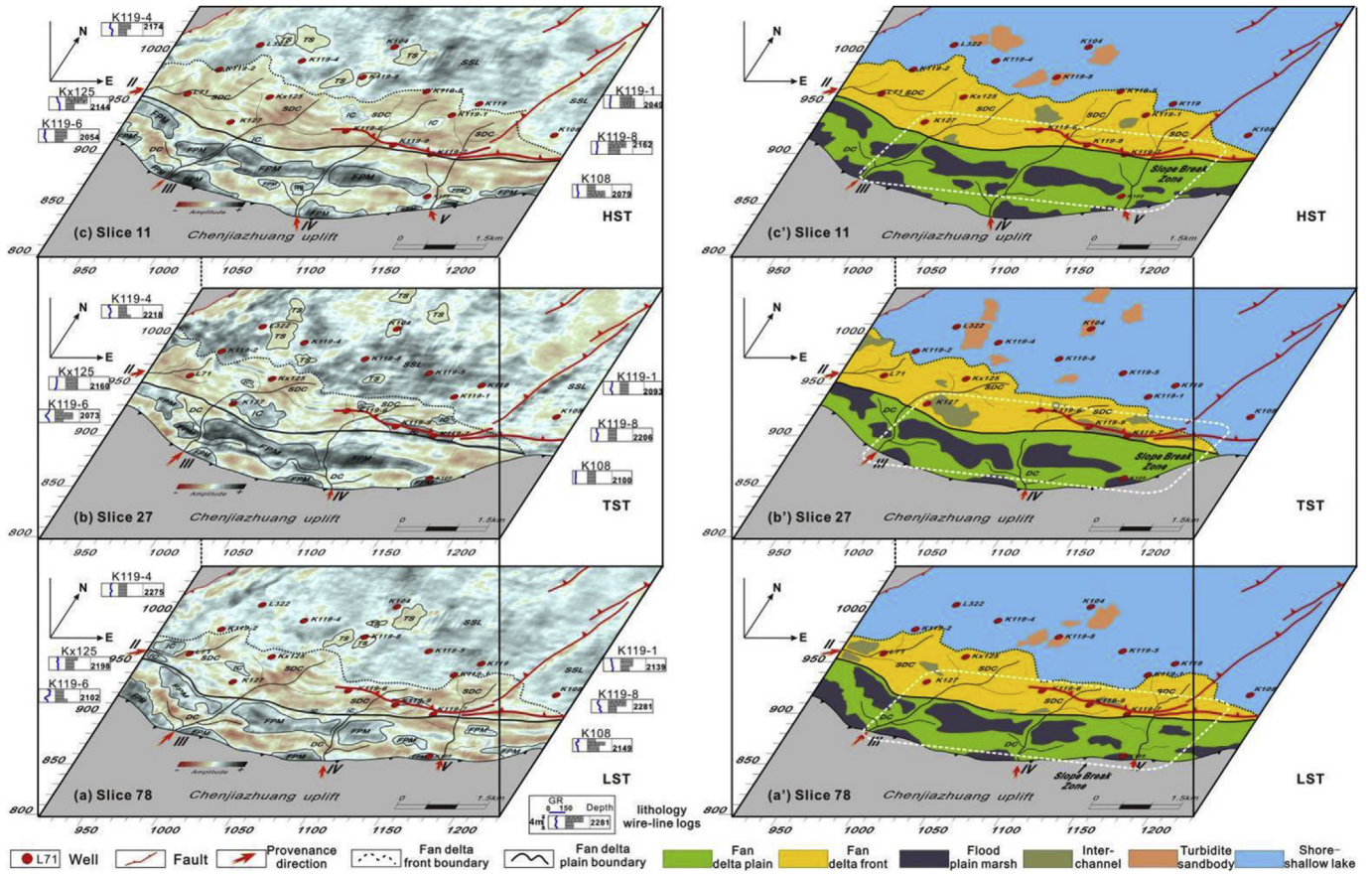

Fig. 13. Three representative stratal slices from SQ2 showing the geomorphologic pattern of the mud-rich fan deltaic system. SSL = shore-shallow lake; TS = turbidite sandbody; SDC = subaqueous distributary channel; IC = interchannel; DC = distributary channel; FPM = flood-plain marsh. The time-interval of each slice is 4 m. (a) Slice 78; (b) Slice 27; (c) Slice 11. See Fig. 4 and 7c to locate the stratal slicings.

5.4.3. Seismic mapping of sequence SQ3

The main depositional system of SQ3 keeps steady. Depositional microfacies include distributary channels, subaqueous distributary channels, interchannels, and sheet sand-bodies (Fig. 14). The main sandbodies are med-thicker, moderate-porosity sheet sandbodies. Fig. 14a, b and c shows typical stratal slices of LST, TST and HST in SQ3.

During the LST, the mixed sand-mud deltas enlarged in the southwest (area is about 7.24 km^2), and were divided into two parts corresponds to valley I and II. The mixed sand-mud fan deltas mainly transported by valley IV and V were located in the south with the area of 15.14 km^2. Fan delta plain subfacies deposited between the first-order and second-order slope break belt, while mud-rich fan delta front subfacies were located under the second-order slope break belt where the microfacies transformed gradually from subaqueous distributary channel to interchannel towards the central area (Fig. 14a, a′). Then, the mud-rich fan delta was shrinking and migrating to the source area in the TST. The fan in southwest reduced to 1.18 km^2, while the southern fan with the area of 5.41 km^2 developed in the Chenjiazhuang Uplift (Fig. 14b, b′). At the HST, the thickness and distribution of sandstones or pebble sandstones increased because of abundant sediments. Thus the fan delta prograded and occupied almost 3/4 of the entire area, and the slump turbidite fan hardly developed (Fig. 14c, c′).

Within sequence SQ3, the fan size increased and the lake shrunk from the lowstand to highstand periods. As the control of slope break belt weakened, sand content of plain facies was higher than the front facies belt, and lithological composition gave priority to frequent sand mud interbeds, which experienced long-distance transport and reworkinng by currents and waves usually with high textural and compositional maturity (Coleman and Prior, 1986). The related fan-deltaic sand-bodes of HST are potential good hydrocarbon reservoirs in sequence SQ3.

6. Dispersal pattern of “source-to-sink” systems

Sediment distribution in the source-to-sink system corresponds to, ‘the sediment routing system’, which often is described in terms of dynamic processes and feedback mechanisms between the various autogenic and allogenic forcing conditions that govern sediment dispersal in erosional-depositional systems (Allen and Hovius, 1998; Allen, 2005, 2008a,b; Densmore et al., 2007; Sømme et al., 2009, 2013; Sømme and Jackson, 2013; Prizomwala et al., 2014). The evolution of system is reflected by morphological modification within one or several adjacent segments (Sømme et al., 2009). Paleogeomorphology is a composite response of what a study area has experienced, including structural deformation, depositional fill, differential compaction, weathering, and erosion. It is an effective method to understand and predict the sedimentary facies and dispersal pattern of depositional systems. During deposition, the paleogeomorphology, together with sediment supply sources, control the spatial dispersal of the depositional systems within the basin (Martin, 1966; Richards et al., 1998; Zeng and Hentz, 2004; Posamentier, 2004; Posamentier et al., 2007; Masini et al., 2011; Dumont et al., 2012; Zhu et al., 2014a). Thus, paleogeomorphologic restoration is a crucial approach for reconstructing

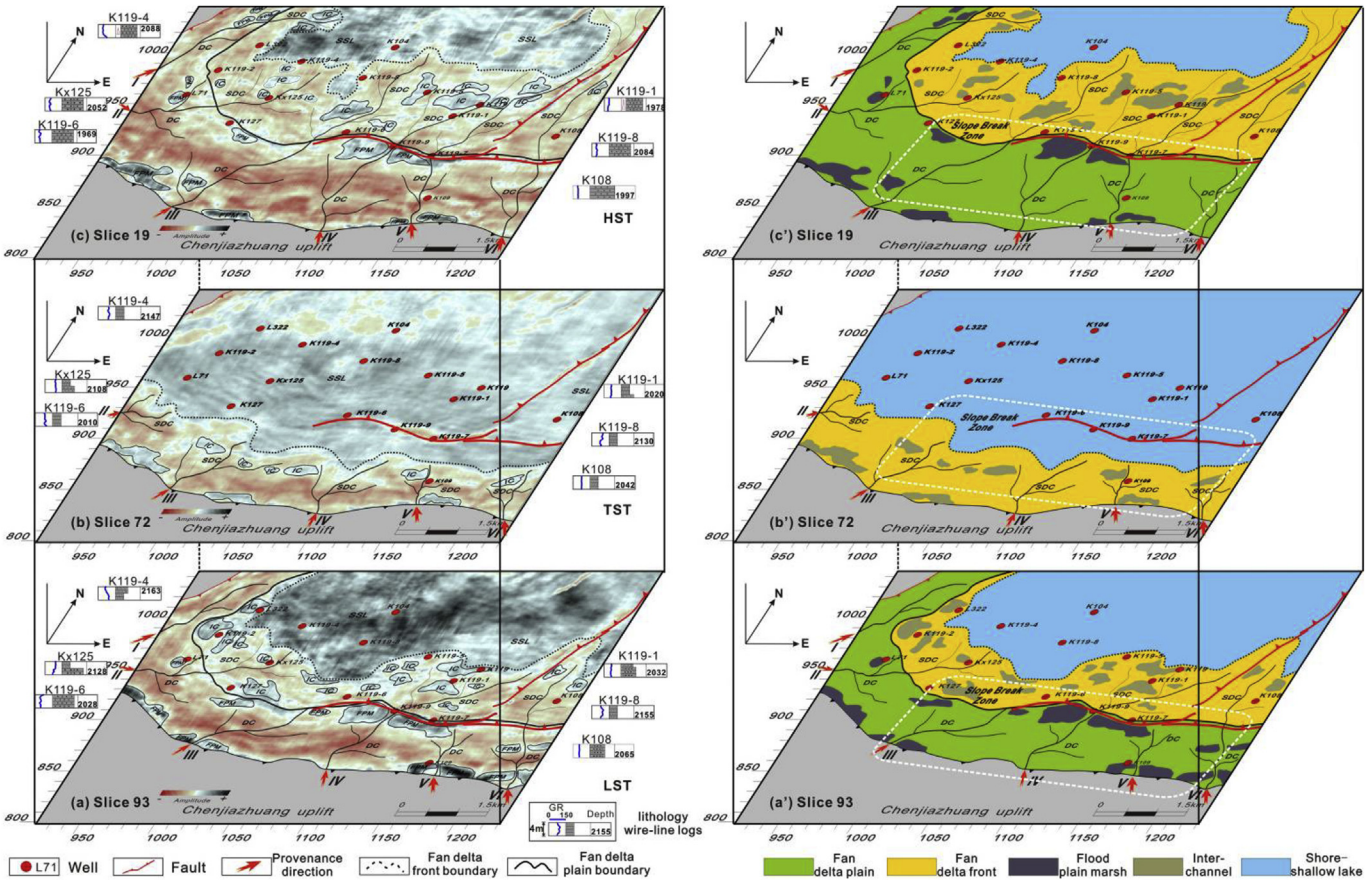

Fig. 14. Three representative stratal slices from SQ3 showing the geomorphologic pattern of the mixed sand-mud fan deltaic system. SSL = shore-shallow lake; SDC = subaqueous distributary channel; IC = interchannel; DC = distributary channel; FPM = flood-plain marsh. The time-interval of each slice is 4 m. (a) Slice 93; (b) Slice 72; (c) Slice 19. See Fig. 4 and 7c to locate the stratal slicings.

depositional systems and predicting reservoir sandstone distribution.

In the study area, the paleogeomorphological architecture is dominated by the Chenjiazhuang Uplift. The topographic features on the map include incised valleys, hill, highland, lowland, slope break belt and sink (Fig. 15a). The positive topographic units control the distribution direction of incised valleys, which determine the direction of sediment transport. The incised valleys and slope break belt distribution showing in Figs. 12–14 have an intimate relationship with belt-shaped or lobe-shaped negative amplitude observed in Fig. 8. These incised valleys converged gradually from source and adjust by slope break belt in sink. The appropriate depositional models of the reservoir sandbodies distribution may determine the appropriate exploration strategies. Based on the above analysis, a conceptual sedimentary model of the "source-to-sink" in research area has been established to show the sediment-dispersal characters under the different types of slope belt, sediment provenance, subsidence rate and their evolution in deposition area (Fig. 15).

1) Southwestern gentle slope system

The western section of Chenjiazhuang uplift, which is composed of Paleozoic marine and marine-terrigenous sediments, and Mesozoic continental volcanic fragment sediments, belongs to peneplain conditions (Fig. 15a). According to the basin-mountain coupling (Contreras and Scholz, 2001; Persano et al., 2006), strong erosion in the western section contributed to high sediment supply corresponding to widely distributed carbonated debris in the southwestern depositional area (Fig. 6a and b). Two inherited valleys I and II with large width-depth ratios and higher delivering capabilities developed in the southwestern gentle slope zone (low gradient about 1.6–3.0°), and the valleys I was the predominant one (Figs. 8 and 15a).

Depositional models of the fan deltas evolved from medium-scale gravel-rich (SQ1) to small-scale mud-rich (SQ2), and lastly to large-scale mixed sand-mud (SQ3) in the southwestern gentle slope system (Figs. 9, 10, 11 and 15b). Within each sequence, the fans of sequence SQ1 mainly developed in the LST with slowly decreasing sizes and numbers from the LST to HST (Figs. 12 and 15b). The fan sizes of the LST and HST of sequence SQ2 were almost the same; while fans in sequence SQ3 mainly occurred in the HST with increasing sizes and numbers from the LST to HST (Figs. 13, 14 and 15b). The favourable reservoir sandstones in the gentle slope system are mainly located in the fan delta front subfacies of HST, sequence SQ1.

2) Southern slope break system

The eastern section of Chenjiazhuang uplift belongs to ravine landform with Archean metamorphic basements and Paleozoic marine-terrigenous sediments (Fig. 15a). Weak erosion in the eastern section led to much more limited sediment supply corresponding to rock fragments predominantly composed of quartz or crystal quartz grains (Fig. 6c, d). Four migrated valleys III ~ VI with smaller width-depth ratios and lower delivering capabilities

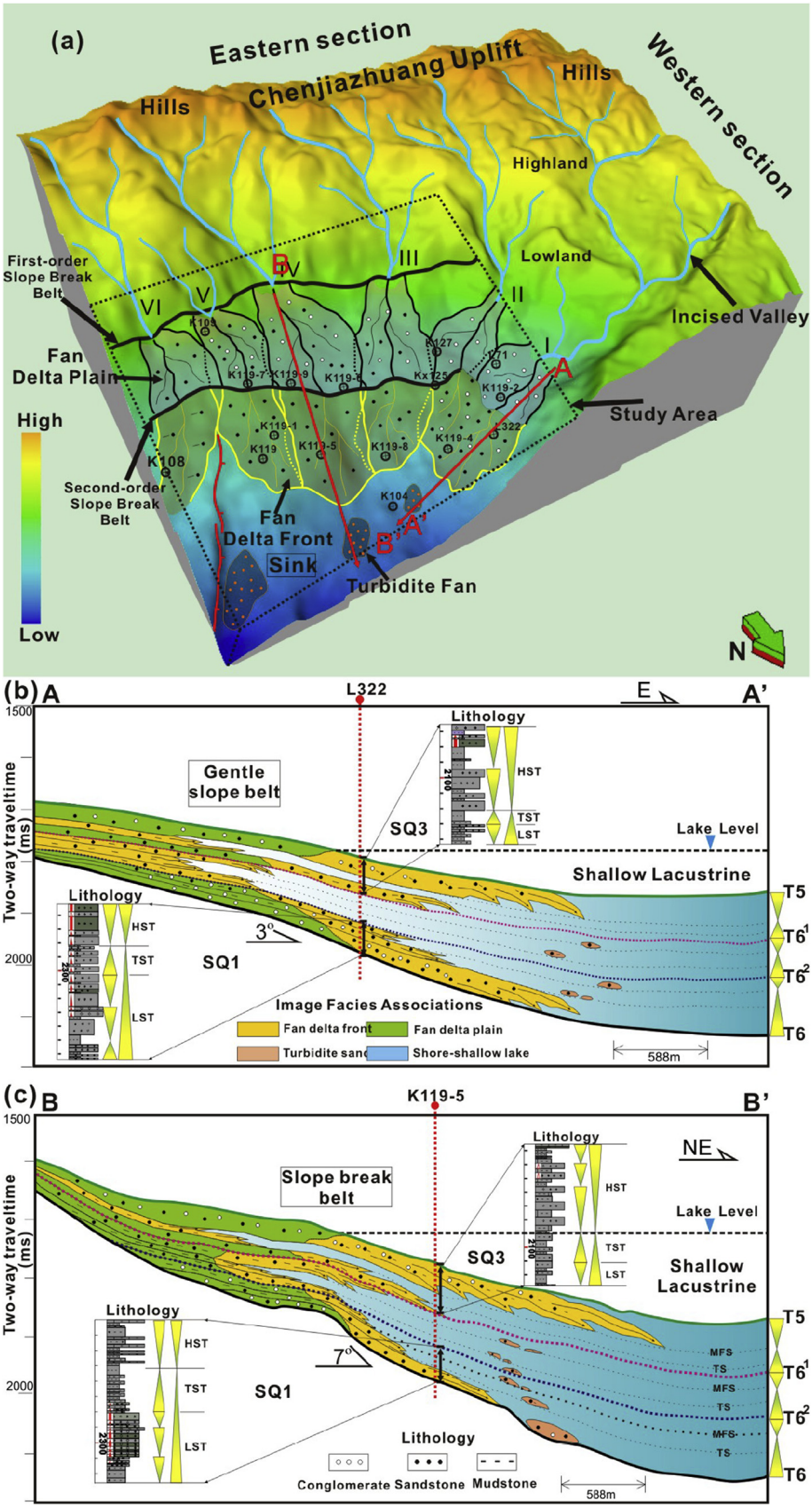

Fig. 15. Sediment-dispersal patterns of "source-to-sink" systems (a) controlled by the 3-D paleo-geomorphological configuration for the third member of Shahejie Formation in the southern slope of Zhanhua Sag. (b) Model of the filling sequence in the gentle slope belt showing the development mechanism of the southwestern fan delta system. The location of the section (A–A′) is shown in Fig. 15a. (c) Model of the filling sequence in the slope break belt showing the development mechanism of the southern fan delta system. The location of the section (B–B′) is shown in Fig. 15a. MFS = Maximum flooding surface; TS = Transgressive Surface. The orientation of Fig. 15a can be seen in the lower right corner.

developed in the southern slope break zone, while the valley IV was the predominant one (Figs. 8 and 15a). And the width-depth ratios of these valleys gradually decreased downstream. In addition, valley systems in the depositional area and two distinct orders of slope break jointly controlled the distribution of sandbodies. The valley shrunk progressively with sedimentary fills resulting in decreasing gradients of the slope break belts with reducing influence on deposition from the sequence SQ1 to SQ3 (Figs. 8 and 15c).

By contrast, the fan delta of southern slope break system changed from sand-rich in SQ1 to mud-rich in SQ2, and then to mixed sand-mud in SQ3 (Figs. 9, 10, 11 and 15c). The sand-rich fan delta system in the sequence SQ1, which led to high gradient (5.8–7.0°) at the second-order slope break point, was related to the slope break belt in the southern zone that. And this fan delta system was dominated by several filling sequences of active fluvial channels with a general coarsening-upwards trend (Fig. 15c). The fans of sequence SQ1 mainly developed in the LST, which decreased obviously in sizes and numbers from the LST to HST (Fig. 12). As a result, the reservoir sandstones under the second-order slope break belt in the LST of SQ1 had good reservoir quality and contained less conglomerate and deformation structures (Figs. 4a, 5 and 6). Meanwhile, the fan-deltaic sand-bodies of HST of sequence SQ3 remained potential good exploration targets (Figs. 4a and 14).

3) Spatial-temporal evolution of source-to-sink systems

Sediment distribution in source-to-sink systems are dependent on a number of variation such as climate, tectonism and drainage basin morphology and some elements varying with time and period of investigation (Sømme et al., 2009). By studying the Chenjiazhuang uplift basements, slope types, morphological relationships and sediment distribution patterns of the third member of Eocene Shahejie Formation in the source-to-sink systems of Zhanhua Sag, several points can be observed from this study. (1) Incised valley-slope break storage related to slope current patterns and valley morphology (width, depth) is directly connected with the size and gradient of the catchment (Fig. 8). (2) The depositional environments of these sequences evolved from medium-scale gravel- or sand-rich fan delta and turbidite (SQ1) to small-scale mud-rich fan delta and turdidite (SQ2), and lastly to large-scale mixed sand-mud fan delta systems (SQ3) (Figs. 9–11). (3) The spatial and temporal evolution of fan sizes and reservoir quality were caused by the lowstand, transgressive, and highstand periods that occurred within the third member of Shahejie Formation, para-second-order sequence during the deposition of the three third-order sequences (SQ1, SQ2, and SQ3) (Figs. 12–14).

Favourable exploration prediction in ancient source-to-sink systems is based on the generic relationship between segments and different types of systems. In the subsurface, where assessment of lithology and reservoir quality is essential for exploration success, a thorough source-to-sink analysis provides a qualified tool by which uncertainty and risk can be reduced for area selection. However, new technology (stratal slice) and testing data (well and seismic) should be taken when predicting systems deposited under different controlling conditions. More research is required prior to selecting an exploration target of the southern fan under the second-order slope break belt in the LST of SQ1 suggested by the analysis above.

7. Conclusions and suggestions

Integration of sequence stratigraphy and seismic geomorphology made it possible for a 3-D facies architecture analysis and the mapping sediment-dispersal patterns of the third member of Eocene Shahejie Formation in the slope system of Zhanhua Sag, Bohai Bay Basin. The following conclusions can be drawn from this study.

1) The third member of the Shahejie Formation (Es_3), a para-second-order sequence, can be subdivided into three third-order sequences, namely SQ1, SQ2 and SQ3 from base to top, which correspond to the lowstand, transgressive, and highstand periods of the Es_3 respectively.
2) Sediments in the Es_3 sequences were delivered from the Chenjiazhuang Uplift via six major incised valleys, four of them (migrated valley III, IV, V and VI) associated with slope-break belt in the southern zone, and others (inherited valley I and II) with large width-depth ratios in the southwestern gentle slope zone. Seismic stratal slices reveal the incised valley shrunk progressively with sedimentary fills resulting in decreasing gradients of the slope break belts with reducing influence on deposition from the sequence SQ1 to SQ3.
3) According to the depositional systems analysis, the depositional environments of these sequences evolved from medium-scale gravel- or sand-rich fan delta and turbidite (SQ1) to small-scale mud-rich fan delta and turdidite (SQ2), and lastly to large-scale mixed sand-mud fan delta systems (SQ3). Especially, during sequence SQ1 with favourable exploration, the gravel-rich fan delta system was distributed in the southwestern gentle slope zone, and the sand-rich fan delta system was distributed in the southern slope break zone.
4) High-resolution sediment-dispersal patterns showed that the fans of sequence SQ1 mainly developed in the LST, which decreased in sizes and numbers from the LST to HST. The fan sizes of the LST and HST of sequence SQ2 were almost the same; while fans in sequence SQ3 mainly occurred in the HST with increasing sizes and numbers from the LST to HST. The spatial and temporal evolution of fan size and reservoir characteristics during the deposition of the three third-order sequences (SQ1, SQ2, and SQ3) were caused by the lowstand, transgressive, and highstand periods that occurred within the para-second-order sequence.
5) Dispersal pattern of the “source-to-sink” system shows sediment-dispersal characteristics with different types of slope belts, sediment provenance, subsidence rate and their evolution in the deposition area, which should serve as a useful reference for the evaluation of hydrocarbon reservoirs in the study area.

In addition, important factors of obtaining the excellent stratal slices include the high quality seismic data and relatively simple structures. In the stratal slices analysis, integration of seismic profiles and other types of data (core, thin section, well logging, and geophysical response, etc), ultimately interpretation of fan delta in slope systems are most reasonable in the study area.

Acknowledgments

This study is supported by the National Natural Science Foundation of China (NSFC) programs (No. 41272133), the National Basic Research Program of China (973 Program) (No. 2011CB201104), and Major National Science and Technology Programs in the “Twelfth Five-Year” Plan period (No. 2011ZX05001-002-01). The authors wish to thank Austin Geo-Modeling, Inc. for providing the Recon and Recon StratalSlice software as well as Landmark Graphics Corporation for providing the software used in this study. We are grateful to the anonymous reviewers and Octavian Catuneanu, the Editor-in-Chief of Marine and Petroleum Geology, for their constructive comments and suggestions, which have greatly improved the manuscript. Finally, we would like to thank Sinopec Shengli Oilfield Company for their support and permission to use

industry data for this research.

References

Abdel-Fattah, Z.A., Kora, M.A., Ayyad, S.N., 2013. Facies architecture and depositional development of Middle Miocene carbonate strata at Siwa Oasis, Northwestern Egypt. Facies 59, 505–528.

Alfaro, E., Holz, M., 2014. Seismic geomorphological analysis of deepwater gravity-driven deposits on a slope system of the southern Colombian Caribbean margin. Mar. Pet. Geol. 57, 294–311.

Allen, P.A., 2005. Striking a chord. Nature 434, 961.

Allen, P.A., 2008a. From landscapes into geological history. Nature 451, 274–276.

Allen, P.A., 2008b. Time scales of tectonic landscapes and their sediment routing systems. In: Gallagher, K., Jones, S.J., Wainwright, J. (Eds.), Landscape Evolution: Denudation, Climate and Tectonics over Different Time and Space Scales. Geological Society, London, Special Publications 296, pp. 7–28.

Allen, P.A., Hovius, N., 1998. Sediment supply from landslide-dominated catchments: implications for basin-margin fans. Basin Res. 10, 19–35.

Carter, D.C., 2003. 3-D seismic geomorphology: insights into fluvial reservoir deposition and performance, Widuri field, Java Sea. AAPG Bull. 87, 909–934.

Catuneanu, O., 2002. Sequence stratigraphy of clastic systems: concepts, merits, and pitfalls. J. Afr. Earth Sci. 35, 1–43.

Catuneanu, O., 2006. Principles of Sequence Stratigraphy. Elsevier, Amsterdam.

Chen, C.M., Huang, J.K., Chen, J.S., Tian, X.Y., Chen, R.J., Li, L., 1981. Evolution of sedimentary tectonics of Bohai rift system and its bearing on hydrocarbon accumulation. Sci. China, Ser.A 24, 521–529.

Chen, D.X., Pang, X.Q., Jiang, Z.X., Zeng, J.H., Qiu, N.S., Li, M.W., 2009. Reservoir characteristics and their effects on hydrocarbon accumulation in lacustrine turbidites in the Jiyang Super-depression, Bohai Bay Basin, China. Mar. Pet. Geol. 26, 149–162.

Chen, S., Wang, H., Wu, Y.P., Huang, C.Y., Wang, J.H., Xiang, X.M., Ren, X.M., 2014. Stratigraphic architecture and vertical evolution of various types of structural slope breaks in Paleogene Qikou sag, Bohai Bay Basin, Northeastern China. J. Pet. Sci. Eng. 122, 567–584.

Chopra, S., Alexeev, V., Pruden, D., 2004. Non-linearity in multi-attribute analysis-tackling. First Break 22, 43–48.

Coe, A.L., Bosence, D.W.J., Church, K.D., Flint, S.S., Howell, J.A., Wilson, R.C.L., 2003. The Sedimentary Record of Sea-level Change. Cambridge University Press, London, pp. 58–73.

Coleman, J.M., Prior, D.B., 1986. Deltaic sand bodies. In: Continuing Education Course Note Series, 15. AAPG Department of Education, pp. 1–67.

Coleou, T., Poupon, M., Azbel, K., 2003. Unsupervised seismic facies classification: a review and comparison of techniques and implementation. Lead. Edge 22, 942–953.

Contreras, J., Scholz, C.H., 2001. Evolution of stratigraphic sequences in multi-segmented continental rift basins: comparison of computer models with the basins of the East African rift system. AAPG Bull. 85, 1565–1581.

Cross, T.A., Lessenger, M.A., 1998. Sediment volume partitioning: Rational for stratigraphic model evaluation and high-resolution stratigraphic correlation. In: Gradstein, F.M., Sandvisk, K.O., Milton, N.J. (Eds.), Sequence Stratigraphy Concepts and Applications. NPF Special Publication 8, pp. 171–195.

Dalla Valle, G., Gamberi, F., Rocchini, P., Minisini, D., Errera, A., Baglioni, L., Trincardi, F., 2013. 3D seismic geomorphology of mass transport complexes in a foredeep basin: examples from the Pleistocene of the Central Adriatic Basin (Mediterranean Sea). Sediment. Geol. 294, 127–141.

Densmore, A.L., Allen, P.A., Simpson, G., 2007. Development and response of a coupled catchment fan system under changing tectonic and climatic forcing. J. Geophys. Res. Earth Surf. 112, 16.

Dong, Y.L., Zhu, X.M., Xian, B.Z., Cheng, K.N., Wang, P., 2014. Mapping sediment-dispersal characteristics using seismic geomorphology: late paleogene to neogene, Qinan sSag, Huanghua depression, China. Mar. Pet. Geol. 54, 180–197.

Dumont, T., Schwartz, S., Guillot, S., Simon-Labric, T., Tricart, P., Jourdan, S., 2012. Structural and sedimentary records of the Oligocene revolution in the Western Alpine arc. J. Geodyn. 56–57, 18–38.

Feng, Y.L., Zhou, H.M., Li, S.T., Liu, W.H., Dong, Y.X., Cao, Z.H., 2004. Sequence types and structural characteristics in congtinental rift-subsidence basins (in Chinese with English abstract). Geol. Rev. 50, 43–49.

Feng, Y.L., Xu, X.S., 2006. Syndepositional structural slope-break zone controls on lithologic reservoirs—a case from Paleogene Bohai Bay Basin (in Chinese with English abstract). Pet. Explor. Dev. 33, 22–25.

Hampson, G.J., Steel, R.J., Burgess, P.M., Dalrymple, R.W., 2008. Recent Advances in Models of Siliciclastic Shallow-Marine Stratigraphy. SEPM Special Publication 90, p. 498.

Hao, F., Zhou, X.H., Zhu, Y.M., Zou, H.Y., Yang, Y.Y., 2010. Charging of oil fields surrounding the Shaleitian uplift from multiple source rock intervals and generative kitchens, Bohai Bay basin, China. Mar. Pet. Geol. 27, 1910–1926.

Hou, G.T., Qian, X.L., Cai, D.S., 2001. The tectonic evolution of Bohai basin in Mesozoic and Cenozoic Time (in Chinese with English abstract). Univ. Pekin. Acta Sci. Nat. 37, 845–851.

Huang, C.Y., Wang, H., Wu, Y.P., Wang, J.H., Chen, S., Ren, P.G., Liu, Y.T., Zhao, S.E., Xia, C.Y., 2012. Genetic types and sequence stratigraphy models of Palaeogene slope break belts in Qikou Sag, Huanghua depression, Bohai Bay Basin, Eastern China. Sediment. Geol. 261, 65–75.

James, H., Peloso, A., Wang, J., 2002. Volume interpretation of multi-attribute 3D surveys. First Break 20, 176–180.

Jiang, S., Sverre, H., Wang, H., Lu, Y.C., Ren, J.Y., Cai, D.S., Feng, Y.L., Paul, W., 2013. Sequence-stratigraphic architectures and sand-body distribution in Cenozoic rifted lacustrine basins, east China. AAPG Bull. 97, 1447–1475.

Jiu, K., Ding, W.L., Huang, W.H., Zhang, Y.Q., Zhao, S., Hu, L.J., 2013. Fractures of lacustrine shale reservoirs, the Zhanhua Depression in the Bohai Bay Basin, eastern China. Mar. Pet. Geol. 48, 113–123.

Kashihara, K., Tsuji, T., 2010. Improvement in facies discrimination using multiple seismic attributes for permeability modelling of the Athabasca Oil Sands, Canada. Explor. Geophys. 41, 80–87.

Khan, Z.A., Tewari, R.C., 2011. Paleochannel and paleohydrology of a Middle Siwalik (Pliocene) fluvial system, northern India. J. Earth Syst. Sci. 120, 531–543.

Lee, K., Royhan Gani, M., McMechan, G.A., Bhattacharya, J.P., Nyman, S.L., Zeng, X.X., 2007. Three- dimensional facies architecture and three-dimensional calcite concretion distributions in a tide-influenced delta front, Wall Creek Member, Frontier Formation, Wyoming. AAPG Bull. 91, 191–214.

Li, J., Tian, B.F., Wang, W.M., Zhao, L.F., Yao, Z.X., 2007. Lateral variation in the sedimentary structure of west Bohai Bay Basin inferred from P-multiple Receiver Functions. Bull. Seismol. Soc. Am. 97, 1355–1363.

Li, S.T., Pan, Y.L., Lu, Y.C., Ren, J.Y., Xie, X.L., Wang, H., 2002. Key technology of prospecting and exploration of subtle traps in lacustrine fault basins: sequence stratigraphic researches on the basis of high resolution seismic survey (in Chinese with English abstract). Earth Science-Journal China Univ. Geosciences 27, 592–598.

Lin, C.S., Pan, Y.L., Xiao, J.X., Kong, F.X., Liu, J.Y., Zheng, H.R., 2000. Structural slope-break zone: key concept for stratigraphic sequence analysis and petroleum forecasting in fault subsidence basin (in Chinese with English abstract). Earth Science-Journal China Univ. Geosciences 25, 260–265.

Lin, C.S., Wang, Q.H., Xiao, J.X., Liu, J.Y., Qiu, Y.G., 2004. Depositional seguence architecture and filling response model of the Cretaceous in the Kuqa depression, the Tarim basin. Sci. China Ser. D-Earth Sci. 47, 86–96.

Liu, E.T., Wang, H., Li, Y., Zhou, W., Leonard, N.D., Lin, Z.L., 2014. Sedimentary characteristics and tectonic setting of sublacustrine fans in a half-graben rift depression, Beibuwan Basin, South China Sea. Mar. Pet. Geol. 52, 9–21.

Ma, X.Y., Liu, H.F., Wang, W.X., Wang, Y.P., 1983. Rifting and extensional tectonics of Meso-Cenozoic in east China (in Chinese with English abstract). Acta Geol. Sin. 57, 22–25.

Mancini, E.A., Obid, J., Badali, M., Liu, K., Parcell, W.C., 2008. Sequence-stratigraphic analysis of Jurassic and Cretaceous strata and petroleum exploration in the central and eastern Gulf coastal plain, United States. AAPG Bull. 92, 1655–1686.

Martin, R., 1966. Paleogeomorphology and its application to exploration for oil and gas (with examples from western Canada). AAPG Bull. 10, 2277–2311.

Masini, E., Manatschal, G., Mohn, G., Ghienne, J.F., Lafont, F., 2011. The tectono-sedimentary evolution of a supra-detachment rift basin at a deep-water magma-poor rifted margin: the example of the Samedan Basin preserved in the Err nappe in SE Switzerland. Basin Res. 23, 652–677.

McPherson, G.J., Shanmugam, G., Moiola, R.J., 1987. Fan-deltas and braid deltas: varieties of coarse-grained deltas. Geol. Soc. Am. Bull. 99, 331–340.

McPherson, J.G., Shanmugam, G., Moiola, R.J., 1988. Fan deltas and braid deltas: conceptual problems. In: Nemec, W., Steel, R.J. (Eds.), Fan Deltas: Sedimentology and Tectonic Settings. Blackie and Son, Glasgow and London, pp. 14–23.

Mitchum, R.M., Van Wagoner, J.C., 1991. High-frequency sequences and their stacking patterns: sequence- stratigraphic evidence of high-frequency eustatic cycles. Sediment. Geol. 70, 131–160.

Morad, S., Ketzer, J.M., De Ros, L.F., 2013. Linking diagenesis to sequence stratigraphy: an integrated tool for understanding and predicting reservoir quality distribution. In: Morad, S., Ketzer, J.M., De Ros, L.F. (Eds.), Linking Diagenesis to Sequence Stratigraphy, International Association of Sedimentologists Special Publication 45, pp. 1–36.

Nordfjord, S., Goff, J.A., Austin Jr., J.A., Sommerfield, C.K., 2005. Seismic geomorphology of buried channel systems on the New Jersey outer shelf: assessing past environmental conditions. Mar. Geol. 214, 339–364.

Orton, G.J., 1988. A spectrum of Middle Ordovician fan deltas and braidplain deltas, North Wales: a consequence of varying fluvial clastic input. In: Nemec, W., Steel, R.J. (Eds.), Fan Deltas: Sedimentology and Tectonic Settings. Blackie and Son, Glasgow and London, pp. 23–49.

Pang, S.Q., Lin, Y., Li, H.Y., 2014. The victory of eighty-first oil fields – Sanhecun oil field record (in chinese). China Energy News 13, 11–17. http://paper.people.com.cn/zgnyb/html/2014-11/17/content_1500559.htm.

Paton, D.A., Van der Spuy, D., Di Primio, R., Horsfield, B., 2008. Tectonically induced adjustment of passive-margin accommodation space; influence on the hydrocarbon potential of the Orange Basin, South Africa. AAPG Bull. 92, 589–609.

Peng, C.S., 2011. Differentiation of mechanisms and models of hydrocarbon accumulation in Chenjiazhuang uplift and its north slope (in Chinese with English abstract). Pet. Geol. Recovery Effic. 18, 16–20.

Persano, C., Bishop, P., Stuart, F.M., 2006. Apatite (U-Th)/He age constraints on the Mesozoic and Cenozoic evolution of the Bathurst region, New South Wales: evidence for antiquity of the continental drainage divide along a passive margin. Aust. J. Earth Sci. 53, 1041–1050.

Posamentier, H.W., Vail, P.R., 1988. Eustatic control on clastic sedimentation: II-Sequence and systems tract models. In: Wilgus, C.H., Hastings, B.S., Kemdall, C. G. St C., Posamentier, H.W., Ross, C.A., Van Wagoner, J.C. (Eds.), Sea-level Changes: an Integrated Approach, SEPM Special Publication 42, pp. 125–154.

Posamentier, H.W., 2001. Seismic geomorphology and depositional systems of deep

water environments: observations from offshore Nigeria, Gulf of Mexico, and Indonesia (abs.). AAPG Annu. Conv. Program 10, 160.
Posamentier, H.W., 2002. Ancient shelf ridges d a potentially significant component of the transgressive systems tract: case study from offshore northwest Java. AAPG Bull. 86, 75–106.
Posamentier, H.W., Kolla, V., 2003. Seismic geomorphology and stratigraphy of depositional elements in deep-water settings. J. Sediment. Res. 73, 367–388.
Posamentier, H.W., 2004. Seismic Geomorphology: imaging elements of depositional systems from shelf to deep basin using 3D seismic data: implications for exploration and development. In: Davies, R.J., Cartwright, J.A., Stewart, S.A., Lappin, M., Underhill, J.R. (Eds.), 3D Seismic Technology: Applications to the Exploration of Sedimentary Basins, Memoirs 29. Geological Society, London, pp. 11–24.
Posamentier, H.W., Davies, R.J., Cartwright, J.A., Wood, L., 2007. Seismic geomorphology d an overview. In: Geological Society (London) Special Publication 277, pp. 1–14.
Postma, G., 1984. Slumps and their deposits in fan delta front and slope. Geology 12, 27–30.
Prather, B.E., 2003. Controls on reservoir distribution, architecture and stratigraphic trapping in slope settings. Mar. Pet. Geol. 20, 529–545.
Prior, D.B., Bornhold, B.D., 1988. Submarine morphology and processes of fjord fan deltas and related high-gradient systems: modern examples from British Columbia. In: Nemec, W., Steel, R.J. (Eds.), Fan Deltas: Sedimentology and Tectonic Settings. Blackie and Son, Glasgow and London, pp. 125–143.
Prizomwala, S.P., Bhatt, Nilesh, Basavaiah, N., 2014. Provenance discrimination and Source-to-Sink studies from a dryland fluvial regime: an example from Kachchh, western India. Int. J. Sediment Res. 29, 99–109.
Qi, J.F., Yang, Q., 2010. Cenozoic structural deformation and dynamic processes of the Bohai Bay basin province, China. Mar. Pet. Geol. 27, 757–771.
Raeesi, M., Moradzadeh, A., Ardejani, F.D., Rahimi, M., 2012. Classification and identification of hydrocarbon reservoir lithofacies and their heterogeneity using seismic attributes, logs data and artificial neural networks. J. Pet. Sci. Eng. 82–83, 151–165.
Ren, J., Tamaki, K., Li, S., Zhang, J., 2002. Late Mesozoic and Cenozoic rifting and its dynamic setting in eastern China and adjacent areas. Tectonophysics 344, 175–205.
Richards, M., Bowman, M., Reading, H., 1998. Submarine-fan systems i: characterization and stratigraphic prediction. Mar. Pet. Geol. 15, 689–717.
Royhan Gani, M., Mustafa Alam, M., 2004. Fluvial facies architecture in small-scale river systems in the Upper Dupi Tila Formation, northeast Bengal Basin, Bangladesh. J. Asian Earth Sci. 24, 225–236.
Sech, R.P., Jackson, M.D., Hampson, G.J., 2009. Three-dimensional modeling of a shoreface-shelf parasequence reservoir analog: part 1. Surface-based modeling to capture high-resolution facies architecture. AAPG Bull. 93, 1155–1181.
Shanley, K.W., McCabe, P.J., 1991. Predicting facies architecture through sequence stratigraphy - an example from the Kaiparowits Plateau, Utah. Geology 19, 742–745.
Shanley, K.W., McCabe, P.J., 1994. Perspectives on the sequence stratigraphy of continental strata. AAPG Bull. 78, 544–568.
Shi, D.S., Li, M.W., Pang, X.Q., Chen, D.X., Zhang, S.W., Wang, Y.S., Jin, Q., 2005. Fault-fracture mesh petroleum plays in the Zhanhua Depression, Bohai Bay Basin: Part 2. Oil-source correlation and secondary migration mechanisms. Org. Geochem. 36, 203–223.
Sømme, T.O., Helland-Hansen, W., Martinsen, O.J., Thurmond, J.B., 2009. Relationships between morphological and sedimentological parameters in source-to-sink systems: a basis for predicting semi-quantitative characteristics in subsurface systems. Basin Res. 21, 361–387.
Sømme, T.O., Jackson, C.A.-L., Vaksdal, M., 2013. Source-to-sink analysis of ancient sedimentary systems using a subsurface case study from the Møre - Trøndelag area of southern Norway: Part 1 – depositional setting and fan evolution. Basin Res. 25, 489–511.
Sømme, T.O., Jackson, C.A.-L., 2013. Source-to-Sink analysis of ancient sedimentary systems using a subsurface case study from the Møre – Trøndelag area of Southern Norway: part 2 – sediment dispersal and forcing mechanisms. Basin Res. 25, 512–531.
Stuart, J.Y., Huuse, M., 2012. 3D seismic geomorphology of a large Plio-Pleistocene delta – 'Bright spots' and contourites in the Southern North Sea. Mar. Pet. Geol. 38, 143–157.
Su, J.B., Zhu, W.B., Wei, J., Xu, L.M., Yang, Y.F., Wang, Z.Q., Zhang, Z.Y., 2011. Fault growth and linkage: implications for tectono-sedimentary evolution in the Chezhen Basin of Bohai Bay, eastern China. AAPG Bull. 95, 1–26.
Sumner, E.J., Talling, P.J., Amy, L.A., Wynn, R.B., Stevenson, C.J., Frenz, M., 2012. Facies architecture of individual basin-plain turbidites: comparison with existing models and implications for flow processes. Sedimentology 59, 1850–1887.
Tian, Z.Y., Han, P., Xu, K.D., 1992. The MesozoiceCenozoic east China rift system. Tectonophysics 208, 341–363.
Tong, K.J., Zhao, C.M., Lu, Z.B., Zhang, Y.C., Zheng, H., Xu, S.N., Wang, J.L., Pan, L.L., 2012. Reservoir evaluation and fracture chracterization of the metamorphic buried hill reservoir in Bohai Bay Basin. Pet. Explor. Dev. 39, 62–69.
Vail, P.R., Audemard, F., Bowman, S.A., Eisner, P.N., Perez-Cruz, C., 1991. The stratigraphic signatures of tectonics, eustasy and sedimentology - an overview. In: Einsele, G., Ricken, W., Seilacher, A. (Eds.), Cycles and Events in Stratigraphy. Springer-Verlag, Berlin Heidelberg, pp. 617–659.
Wang, J.D., 2005. Generation and Aceumulation of Hydroearbon and Tcetonic Evolution of the Buried – Hill in the Jiyang Depression. Ocean University of China, Qindao, China, pp. 12–34.
Wang, Y.H., Liu, Q.H., Zhu, X.M., Zhu, S.F., Jiang, L., Geng, M.Y., Jiang, Y.B., Zhang, Y.L., Liu, Y., 2015. Provenance analyses of the lower third member of paleogene Shahejie Formation in Sanhecun Sub-sag, Zhanhua Sag (in Chinese with English abstract). Geol. J. China Univ. 21, 426–439.
Wang, Y.S., Li, M.W., Pang, X.Q., Zhang, S.W., Shi, D.S., Chen, D.X., 2005. Fault-fracture mesh petroleum plays in the Zhanhua Depression, Bohai Bay Basin: Part 1. Source rock characterization and quantitative assessment. Org. Geochem. 36, 183–202.
Watson, M.P., Hayward, A.B., Parkinson, D.N., Zhang, Z., 1987. Plate tectonic history, basin development and petroleum source rock deposition onshore China. Mar. Pet. Geol. 4, 205–225.
Wen, Z.G., Zhou, D.H., Song, H.X., Li, J.P., Tang, Y.J., 2009. Analysis of hydrocarbon exploration potential in Bozhong depression-compared with Dongying and Zhanhua depressions (in Chinese with English abstract). J. Oil Gas Technol. 31, 55–58.
Wood, M.L., Ethridge, F.G., 1988. Sedimentology and architecture of Gilbert- and mouth bar-type fan deltas, Paradox basin, Colorado. In: Nemec, W., Steel, R.J. (Eds.), Fan Deltas: Sedimentology and Tectonic Settings. Blackie and Son, Glasgow and London, pp. 251–263.
Wood, L.J., 2007. Quantitative seismic geomorphology of Pliocene and Miocene fluvial systems in the northern Gulf of Mexico, USA. J. Sediment. Res. 77, 713–730.
Wright, V.P., Marriot, S.B., 1993. The sequence stratigraphy of fluvial depositional systems: the role of floodplain sediment storage. Sediment. Geol. 86, 203–210.
Ye, H., Shedlock, K.M., Hellinger, S.J., Sclater, J.C., 1985. The North China basin: an example of a Cenozoic rifted intraplate basin. Tectonics 4, 153–169.
Zeng, H.L., Backus, M.M., Barrow, K.T., Tyler, N., 1998a. Stratal slicing: part I: Realistic 3-D seismic model. Geophysics 63, 502–513.
Zeng, H.L., Henry, S.C., Riola, J.P., 1998b. Stratal slicing: part II: Real 3-D seismic data. Geophysics 63, 514–522.
Zeng, H.L., 2001. From seismic stratigraphy to seismic sedimentology: a sensible transition. Gulf Coast Assoc. Geol. Soc. 51, 413–420.
Zeng, H.L., Hentz, T.F., 2004. High-frequency sequence stratigraphy from seismic sedimentology: applied to Miocene, Vermilion Block 50, Tiger Shoal area, offshore Louisiana. AAPG Bull. 88, 153–174.
Zeng, H.L., Zhu, X.M., Zhu, R.K., Zhang, Q.S., 2012. Guidelines for seismic sedimentologic study in non-marine postrift basins. Pet. Explor. Dev. 39, 295–304.
Zhao, L., Zheng, T.Y., 2005. Seismic structure of the Bohai Bay Basin, northern China: implications for basin evolution. Earth Planet. Sci. Lett. 9, 9–22.
Zhang, S.W., Zhang, L.Y., Bao, Y.S., Li, X.Y., Liu, Q., Li, J.Y., Yin, Y., Zhu, R.F., Zhang, S.C., 2012. Formation fluid characteristics and hydrocarbon accumulation in the Dongying sag, Shengli Oilfield. Pet. Explor. Dev. 39, 423–435.
Zhang, S.W., Wang, Y.S., Shi, D.S., Xu, H.M., Pang, X.Q., Li, M.W., 2004. Fault-fracture mesh petroleum plays in the Jiyang Superdepression of the Bohai Bay Basin, eastern China. Mar. Pet. Geol. 21, 651–668.
Zhu, G.Y., Jin, Q., Zhang, S.C., Guo, C.C., Zhang, S.W., Zhang, L.Y., 2004. Study on complex hydrocarbon accumulation and reservoir formation in the rift lacustrine basin. Acta Pet. Sin. 25, 12–18.
Zhu, H.T., Yang, X.H., Zhou, X.H., Liu, K.Y., 2014a. Three-dimensional facies architecture analysis using sequence stratigraphy and seismic sedimentology: example from the Paleogene Dongying Formation in the BZ3-1 block of the Bozhong Sag, Bohai Bay Basin, China. Mar. Pet. Geol. 51, 20–33.
Zhu, H.T., Yang, X.H., Liu, K.Y., Zhou, X.H., 2014b. Seismic-based sediment provenance analysis in continental lacustrine rift basins: an example from the Bohai Bay Basin, China. AAPG Bull. 98, 1995–2018.